cloned into the pTSC21 plasmid for expression under the control of the mouse Thy-1 promoter. The same promoter was used to express APP with the KM670/671NL "Swedish" mutation in APP23 mice as described previously (Sturchler-Pierrat et al., 1997). The mice were on a C57BL/6 background and hemizygous for the transgene. They were killed, and tissues were prepared as described previously (Abramowski et al., 2008). All animal experiments were in compliance with protocols approved by the Swiss Animal Care and Use Committees.

Biochemical assays. Brain samples were processed and analyzed for Aβ peptides [immunoprecipitation of Aβ and Western blotting or matrix-assisted laser desorption ionization time-of-flight (MALDI-TOF), electrochemiluminescence-linked immunoassay (MSD 96-Well Multi-Array Human (6E10) $A\beta_{40}$ or $A\beta_{42}$ Ultra-Sensitive kits; Meso Scale Discovery)] as described previously (Abramowski et al., 2008).

Sequential Aβ extraction and immunoprecipitation. For Triton X-100 (TX-100) (93418; Fluka/Sigma-Aldrich) extraction, forebrain homogenates were extracted with 1% TX-100 in TBS–Complete for 15 min on ice and ultracentrifuged (100,000 × *g*, 4°C, 15 min), and the clear supernatants were immunoprecipitated as described below. The pellets were used for further SDS extraction. Subsequently, TX-100 pellets were extracted with SDS in TBS–Complete for 15 min at room temperature either with 1 or 2% SDS. The extracts with 1% SDS were diluted after extraction to 0.1% final SDS concentration with TBS–Complete. After ultracentrifugation (100,000 × *g*, 4°C, 15 min), immunoprecipitation from the clear supernatant was done with 6E10 and the pellets were used for further formic acid extraction. Extracts with 2% SDS were ultracentrifuged (100,000 × *g*, 20°C, 15 min), and the supernatants were subsequently diluted to a final 0.1% SDS concentration. These SDS extracts and formic acid-extracted pellets were immunoprecipitated with 4G8 (SIG-39200; Covance) only. SDS pellets were extracted with 70% formic acid for 15 min at room temperature, neutralized with 19 vol (v/v) 1 M Tris-base/1% TX-100/Complete and ultracentrifuged (100,000 × *g*, 4°C, 15 min). The clear supernatant was used for immunoprecipitation, and the pellet was discarded. Aβ standards were prepared by spiking synthetic Aβ peptides to nontransgenic forebrain extracts processed the same as described for the samples.

All extracts were either immunoprecipitated with 6E10 (SIG-39300; Covance) bound to Dynabeads Protein G (100.03; Invitrogen) or 4G8 (SIG-39200; Covance) bound to Protein G-Sepharose 4 Fast Flow (17-0618-01; GE Healthcare Life Sciences) and incubated overnight at 4°C on end-over-end rotor. After incubation, the supernatants were removed, and the Dynabeads were washed with TBS–Complete/1% NP-40, then with 10 mM Tris-HCl, pH 7.5, and finally with 1 mM Tris-HCl, pH 7.5. Sepharose beads were washed once with 20 mM Tris-HCl, pH 7.5. Samples were boiled with sample buffer for 5 min at 95°C and analyzed on Western blot.

Sequential immunoprecipitation. For sequential immunoprecipitation, forebrain homogenates were extracted with 1% TX-100 as described above. To the extract, α Aβ (N3pE) antibody (18591; IBL)-bound Dynabeads Protein G were added and incubated overnight at 4°C on end-over-end rotor. After incubation, the supernatants were transferred to fresh tubes and the extracts were immunoprecipitated a second time with 6E10 antibody bound to Dynabeads Protein G as described above. The beads from both immunoprecipitations were processed the same as described above.

Western blot. For Aβ peptide determination on Western blot, forebrain homogenates were separated on a 13% Tris-bicine gel with 8 M urea as described previously (Klafki et al., 1996; Staufenbiel and Paganetti, 2000). In this gel system, the different Aβ peptides are well separated. Proteins were transferred to Immobilon-P membranes (Millipore). Aβ peptides were heat fixed to the membrane by boiling for 3 min in PBS (P4417; Sigma-Aldrich). Aβ peptides were detected with 6E10 (SIG-39300; Covance) or N3pE Aβ with α Aβ (N3pE) antibody (18591; IBL). Proteins were detected by visualizing chemiluminescence (ECL Advance or ECL Plus; GE Healthcare) on autoradiographic films (Hyperfilm ECL; GE Healthcare).

In situ *hybridization.* The spatial distribution pattern of SPENK-$A\beta_{40}$ or SPENK-$A\beta_{42}$ transgene expression was determined by *in situ* hybridization (Sturchler-Pierrat et al., 1997) with a ^{33}P-labeled oligonucleotide (5′-CGCCCACCATGAGTCCAATGATTGCACCTTTGTTTGAACC-3′). The probe binds entirely within the Aβ-coding part. It contains four mismatches compared with the mouse APP sequence and did not cross-react with mouse APP RNA.

RNA quantification. Total RNA extraction, cDNA synthesis, and real-time PCR gene expression analysis and quantification were done as described by Reichwald et al. (2009). TaqMan Gene Expression Assays were ordered from Eurogentec (18s rRNA control kit FAM-TAMRA; RT-CKFT-18s) or designed (SPENK40/42F1: CAG AGG AAG GAC CTC GAA GCT; SPENK40/42R1: AAC AAA GGT GCA ATC ATT GGA CT; MGB Taq40: FAM-TCG ACC TAG ACA ACA CC-MGBNFQ; MGB Taq42: FAM-TCG ACC TAC GCT ATG ACA-MGBNFQ). Real-time PCR quantifications were run in triplicate for each sample and the average determined. Mice were analyzed in groups of 10 per genotype.

Neuropathology and immunocytochemistry. Tissue fixation, sectioning, and processing were done as described previously (Sturchler-Pierrat et al., 1997; Abramowski et al., 2008). Conventional silver staining for axonal neurofilaments was performed with the Bodian method. The Campbell–Switzer silver impregnation was used to stain fibrillar Aβ with high sensitivity (Braak and Braak, 1991; Thal et al., 1999).

Immunohistochemistry was performed for the detection and quantification of Aβ pathology in APP48. Before the use of monoclonal mouse antibodies, 100-μm-thick free-floating sections were incubated with goat anti-mouse IgG for blocking intrinsic mouse IgG (Thal et al., 2007). To detect $A\beta_{1-42}$-positive material, the sections were stained with monoclonal antibodies specifically detecting the C terminus of $A\beta_{42}$ [MBC42 (Yamaguchi et al., 1998); 1/200; formic acid pretreatment; 24 h at 22°C] or with an antibody raised against $A\beta_{17-24}$ (4G8; Covance; 1/5000; formic acid pretreatment; 24 h at 22°C), with an antibody directed against the N terminus of $A\beta_{1-42}$ [AβN1D (Saido et al., 1995); polyclonal rabbit; 1/100; formic acid and microwave pretreatment], and with anti-AβN3pE (polyclonal rabbit; IBL; 1/100; formic acid and microwave pretreatment). To exclude tau and TDP43 pathology, an antibody against abnormal phosphorylated tau protein (AT-8; monoclonal mouse; Thermo Fisher Scientific; 1/1000; 24 h at 22°C) and an antibody against phosphorylated TDP43 (pTDP43: pS409/410-2; Cosmo Bio; 1/10,000; microwave pretreatment) were used. Astrocytes were labeled with an antibody directed against the glial fibrillary acidic protein (GFAP) (polyclonal rabbit; Dako; 1/1000; 24 h at 22°C), microglial cells with *Ricinus communis* agglutinin (RCA) (Vector Laboratories; 1/250; 24 h at 22°C). To test whether APP was present in Aβ aggregates or in plaque-associated dystrophic neurites, antibodies directed against APP were used (22C11; monoclonal mouse; Millipore Bioscience Research Reagents; 1/75; 24 h at 22°C). To identify abnormalities in the neuronal network, sections of each mouse were stained with antibodies against 68 kDa subunits of neurofilament protein (NF-L; SPM 204; Zytomed; 1/100; microwave pretreatment; 24 h at 22°C) and synaptophysin (polyclonal rabbit; Dako; 1/1000; microwave pretreatment). The primary antibodies were detected with a biotinylated secondary antibody and the ABC complex (Biomeda), and visualized with diaminobenzidine-HCl (DAB) (Hsu et al., 1981). Sections were mounted in Eukitt (Kindler). Biotinylated RCA was detected with the ABC complex and visualized with DAB.

For double immunofluorescence, 20-μm-thick free-floating sections were incubated with rabbit Aβ antiserum NT11 and monoclonal antibody (clone AP20; Millipore Bioscience Research Reagents) against microtubule-associated protein 2 (MAP2) as dendritic marker. Alternatively, CD45 monoclonal antibody MCA1031G (Serotec) was used to label microglia cells. Primary antibodies were detected with horseradish peroxidase (HRP)-labeled anti-rabbit IgG (Dako) and HRP-labeled anti-mouse IgG (Dako) secondary antibodies. Signal Amplification has been done by applying Cy3- or FITC-conjugated Tyramide (NEL741; PerkinElmer).

To determine the intracellular location of Aβ-reactive structures, labeling with Aβ antibody 4G8 was colocalized with antibody labeling of different compartmental markers: LAMP-1 (ab62562; Abcam) for late endosomes/lysosomes, EEA1 (ab2900; Abcam) for early endosomes, BiP (anti-KDEL; SPA-827; Stressgen) for post-endoplasmatic reticulum compartments, and TIA-1/TIAR(D-9) (sc-48371; Santa Cruz) for stress granules. Aβ was detected with Cy2-labeled secondary antibodies,

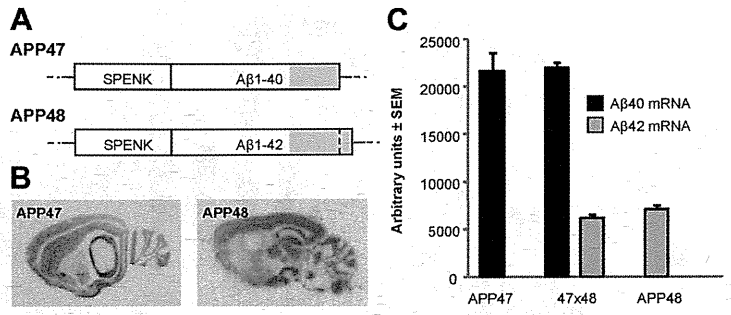

Figure 1. APP47 and APP48 transgenes and brain mRNA expression. ***A***, Schematic representation of the APP47 and APP48 expression constructs. The box represents the translated sequence comprising the cleaved N-terminal signal sequence SPENK (signal peptide preproenkephalin) followed by $A\beta_{1-40}$ or $A\beta_{1-42}$. The gray C-terminal end denotes the hydrophobic amino acid stretch of Aβ, which is approximately one-half of the APP transmembrane region (located in the luminal leaflet of the membrane bilayer). ***B***, *In situ* hybridization to locate the transgene expression in 2-month-old APP47 and APP48 mouse brain. ***C***, Relative transgene mRNA levels in forebrain of female APP47, APP48, and APP47 × APP48 (47 × 48) mice as determined by quantitative PCR. Animals were 2 months of age. Differences between $A\beta_{1-40}$ and $A\beta_{1-42}$ mRNAs were statistically significant (Student's *t* test, two-tailed, $p < 0.0001$), whereas the same mRNAs did not differ significantly ($p > 0.1$) between single- and double-transgenic mice. Error bars indicate SEM.

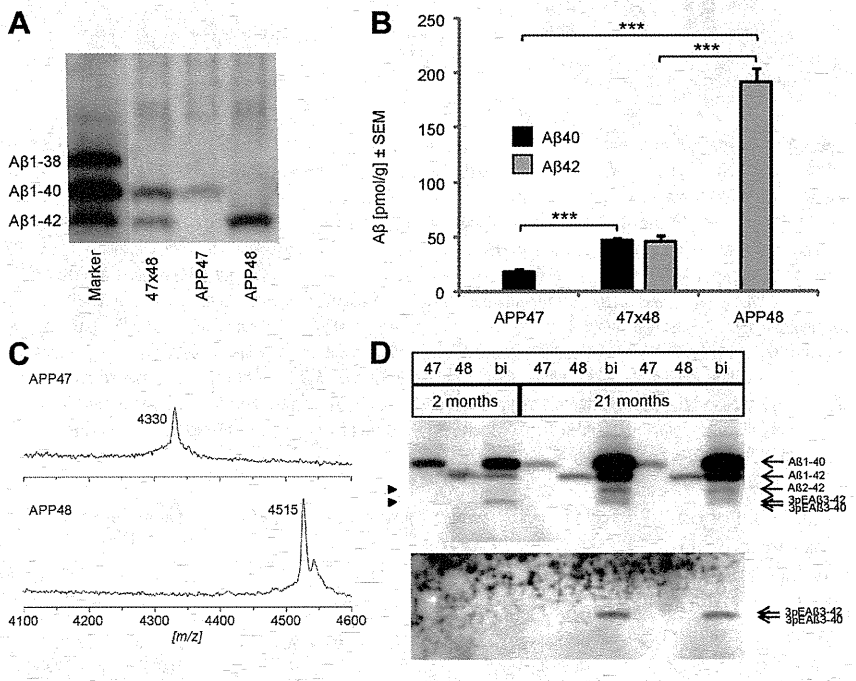

Figure 2. Characterization of human $A\beta_{40}$ and $A\beta_{42}$ peptides in brain. ***A***, Western blot of forebrain homogenates from representative Aβ-expressing mice at 2 months. Female mice are shown, but results were similar for males. Homogenates were dissolved in SDS-sample buffer and run on a SDS/urea gel to separate $A\beta_{1-40}$ and $A\beta_{1-42}$. The gel was overloaded to improve detection. Synthetic Aβ peptides spiked into a nontransgenic mouse brain homogenate are shown on the left. Note that $A\beta_{1-40}$ and $A\beta_{1-42}$ blot with different efficiency and cannot be compared directly. ***B***, Formic acid-extracted total Aβ was quantified by an electrochemoluminescence assay (MSD). Significant differences (Student's *t* test, two-tailed) are indicated by asterisks: $***p < 0.001$. One-way ANOVA and Tukey's test showed a significant difference between $A\beta_{40}$ and $A\beta_{42}$ in APP47 versus APP48 mice ($p < 0.001$) but not within the double-transgenic animals (47 × 48; Student's *t* test, two-tailed, $p = 0.83$). Error bars indicate SEM. ***C***, MALDI spectra of immunoprecipitates with Aβ antibody 6E10 from brain extracts of APP47 and APP48 mice showed peaks at the expected molecular weight of $A\beta_{1-40}$ and $A\beta_{1-42}$, respectively. ***D***, Forebrain homogenates of 2- and 21-month-old APP47, APP48, and APP47 × APP48 (47 × 48) mice were immunoprecipitated with Aβ antibody 6E10, separated on a SDS/urea gel, and detected by Western blotting using an N3pE (pyroglutamate; upper panel) or general (6E10; lower panel) Aβ antibody. The two faster migrating bands are indicated by arrowheads. Pyroglutamate Aβ was detected as a minor portion of the fastest band in aged double-transgenic mice only. The migration positions of synthetic standards are indicated on the right.

whereas the compartmental markers were detected with Cy3-labeled secondary antibodies.

In the event that single-label immunohistochemistry was performed on paraffin sections, a counterstaining with hematoxylin was applied. The immunostained sections were analyzed with a Leica DMLB fluorescence microscope (Leica). Quantification of Aβ pathology in APP48 was performed in the area of the frontocentral neocortex.

Stereology. Six APP48 and six wild-type mice, 18 months of age, were used for stereology. One hundred-micrometer-thick coronal sections were stained with the aldehyde fuchsin–Darrow red method exhibiting a Nissl-like staining pattern of the neurons and the pigment architecture for anatomical parcellation (Braak, 1974). The frontocentral cortex volume for stereology was defined as the volume of the subfields M2, M1, S1 starting at the level of the anterior commissure as described previously (Capetillo-Zarate et al., 2006). The CA1 volume was measured in serial 100-μm-thick sections. Quantification of neurons was performed for the frontocentral cortex and the hippocampal sector CA1, separately, according to the principles of unbiased stereology (Schmitz and Hof, 2000).

The number of specific types of Aβ aggregates in the frontocentral neocortex was counted in accordance with the principles of unbiased stereology.

The relative volume of the forebrain white matter was determined by measuring the area of the Luxol fast blue (LFB)-stained forebrain white matter and the total area of the forebrain in the same section. The percentage of the hemispheres covered by white matter was calculated as follows: Forebrain white matter volume (%) = (forebrain area stained with LFB × 100)/total forebrain area.

Electron microscopy and immuno-electron microscopy. One 100-μm-thick vibratome section of the frontocentral cortex of six 18-month-old wild-type and APP48/167 mice was stained with osmium tetroxide and flat-embedded in Epon (Fluka). A second vibratome section was also stained with osmium tetroxide and then flat embedded in LR-White-Resin (Hard-Grade Acrylic Resin; London Resin Company). A part of the frontocentral cortex covering all six cortical layers was dissected under microscopic control and pasted on Epon blocks with a drop of Epon. Ultrathin sections were cut at 70 nm. Epon sections were block stained with uranyl acetate and lead citrate, and viewed with a Philips EM400T 120 kV. LR-White sections were immunostained with anti-MAB42 antibodies and visualized with anti-mouse secondary antibodies (Aurion ImmunoGold Reagents & Accessories) labeled with 10 nm nanogold particles. Digital pictures were taken.

Rotarod test. To measure motor coordination, 5- to 7-month-old mice were placed on a horizontal cylinder (Ugo Basile; treadmill for mice Typ 7600) rotating at 13 rounds per minute. The time until the mice fell off the cylinder was measured. Three trials were performed on consecutive days. Trials were terminated after a maximum of 120 s.

Statistical analyses. For statistical analysis, we used Student's *t* tests (two-tailed) or ANOVA followed by Tukey's test for pairwise comparison of all groups as indicated in the figure legends. Rotarod data were

analyzed by Mann–Whitney *U* test followed by Tukey's test; $p < 0.05$ was considered significant for all tests; analyses were done with Systat for Windows 11 (Systat Software) or SPSS 16.0 (SPSS).

Results

Within APP, the N terminus of the Aβ peptide is located in the lumen of the intracellular membrane systems, while its C terminus resides in the center of the transmembrane region (Kang et al., 1987). To insert human $A\beta_{1-40}$ or $A\beta_{1-42}$ in the same membrane orientation during translation at the endoplasmic reticulum, cDNA constructs were made encoding the rat preproenkephalin signal sequence (SPENK) in front of both peptides (Fig. 1*A*). *In vitro* translation of these constructs indicated signal sequence cleavage in the presence of microsomes accompanied by an association of the Aβ peptides with the membrane vesicles (data not shown). Studies with transfected HEK cells had shown approximately equal amounts of $A\beta_{1-40}$ remaining associated with cells and released into the culture medium. In contrast, $A\beta_{1-42}$ largely remained cell associated as also noted by others (Maruyama et al., 1995) (our unpublished data). The murine Thy-1 promoter (Lüthi et al., 1997) was used to drive neuronal expression in brain. For both constructs, the lines with the highest brain Aβ concentration were selected for further studies, APP47 ($A\beta_{1-40}$) and APP48 ($A\beta_{1-42}$).

Aβ expression in APP47 and APP48 mice

The spatial transgene expression pattern in brain was analyzed by *in situ* hybridization (Fig. 1*B*). For both APP47 and APP48 mice, prominent labeling was found in cerebral cortex and hippocampus as expected for the Thy-1 promoter. Other regions including thalamus, cerebellum, and some subcortical nuclei also showed substantial expression. Relative transgene mRNA concentrations in forebrain of young (2-month-old) APP47 and APP48 mice are shown in Figure 1*C*. They were approximately threefold higher for APP47 than for APP48. In double transgenic mice, the expression of both constructs remained unchanged indicating that coexpression did not result in detectable interference of the transgenes.

Young mice were analyzed for Aβ peptides using Western blotting of forebrain homogenates dissolved in SDS-sample buffer (Fig. 2*A*). In contrast to the corresponding mRNA, $A\beta_{1-42}$ reached a considerably higher level than $A\beta_{1-40}$, in agreement with its reduced clearance following brain injection of synthetic peptides (Ji et al., 2001). Quantification of the Aβ peptides after formic acid extraction indicated a ~10-fold higher steady-state concentration of $A\beta_{42}$ than $A\beta_{40}$ (Fig. 2*B*). Interestingly, in APP47 × APP48 mice, $A\beta_{42}$ was reduced by ~75% compared with single transgenic mice, while $A\beta_{40}$ was elevated ~2.5-fold. The absolute concentrations of both peptides were very similar, suggestive of an interaction.

The identity of the Aβ peptides in APP47 and APP48 mice was confirmed by MALDI-TOF analysis following immunoprecipitation of SDS-dissolved forebrain extracts (Fig. 2*C*). The molecular weights determined for the Aβ peaks in both transgenic lines were in agreement with the full-length $A\beta_{1-40}$ and $A\beta_{1-42}$ peptides, respectively. These data demonstrate the proper cleavage of the signal sequence. No other Aβ peptides were detectable. SDS gels in addition showed one or two faster migrating bands, most notably in APP47 × APP48 mice, which varied in amount but always remained minor forms (Fig. 2*D*). The upper band comigrated with $A\beta_{2-42}$ and the lower one with $A\beta_{4-40/42}$ and pyroglutamate Aβ ($N3pEA\beta_{3-40/42}$). To further characterize the lower band, Aβ was immunoprecipitated from forebrain homogenates followed by Western blotting with an N3pEAβ antibody. Only

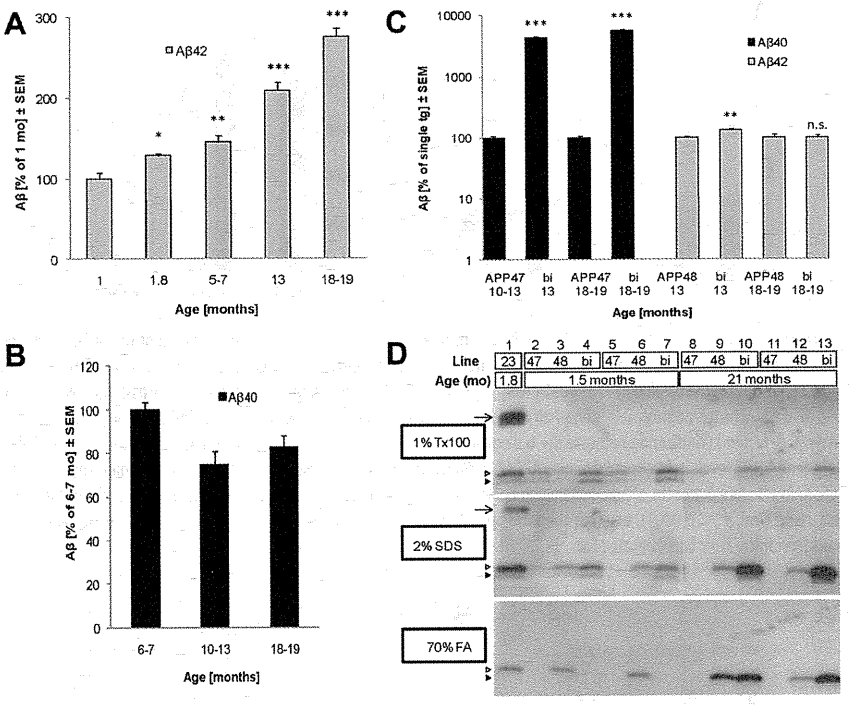

Figure 3. Age-dependent changes and solubility characteristics of brain Aβ in APP47 and APP48 mice. Formic acid-extracted total $A\beta_{40}$ and $A\beta_{42}$ in cerebral cortex was analyzed at the indicated ages using electrochemoluminescence assays. ***A***, The $A\beta_{42}$ concentration in APP48 brain significantly increased with age (Student's *t* test vs 1 month, two-tailed) as indicated by asterisks: $*p < 0.05$, $**p < 0.01$, $***p < 0.001$. Linear regression analysis (regression ANOVA $F_{(1,32)} = 317.7$, $p < 0.001$) indicated age as a strong and linear determinant of $A\beta_{42}$. ***B***, The $A\beta_{40}$ concentration in APP47 mouse brain remained unchanged ($p > 0.05$, Student's *t* test, two-tailed, and linear regression). ***C***, Compared with APP47, $A\beta_{40}$ was considerably elevated in aged APP47 × APP48 mice, whereas $A\beta_{42}$ was not consistently different from APP48 (Student's *t* test vs single-transgenic mice, two-tailed). Error bars indicate SEM. ***D***, Forebrain homogenates of 1.5- and 21-month-old APP47, APP48, and APP47 × APP48 (bi) mice were sequentially extracted with 1% Triton X-100, 2% SDS, and 70% formic acid. Extracts were immunoprecipitated with antibody 4G8 and analyzed by Western blotting with antibody 6E10, both directed against Aβ. A gel without urea was used, which does not separate $A\beta_{1-40}$ and $A\beta_{1-42}$. The faster migrating band corresponds to the truncated Aβ isoforms separated on SDS/urea gels (see above). This band is primarily found in the Triton and SDS extracts from young mice. An extract from a young APP transgenic mouse (APP23) is shown for comparison.

Table 1. Average forebrain weight of APP47, APP48, and double-transgenic mice at 2 and 21 months of age

Age group	Wild type	APP47	APP48	APP47 × APP48
2 months				
Forebrain weight (mg)[a]	164 ± 10	165 ± 9	152 ± 10	152 ± 7
p (vs wild type)*		NS	0.006	0.002
21 months				
Forebrain weight (mg)[a]	161 ± 10	154 ± 9	132 ± 8	131 ± 10
p (vs wild type)*		NS	<0.0001	<0.0001

[a]Shown are mean ± SD.

*Student's *t* test, two-tailed. NS, Nonsignificant.

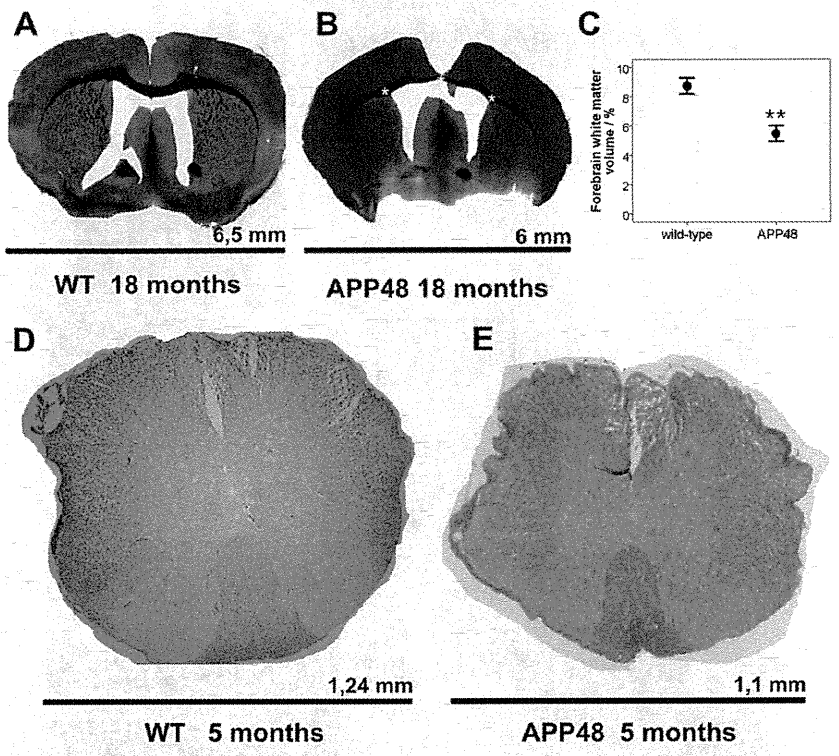

Figure 4. Macroscopic analysis of brains from APP48 mice. The forebrain of APP48 (***B***) mice was ~10% smaller than that of wild-type mice (***A***) as measured by the bi-hemispheric diameter, which is indicated as black bar below the brain section. The relative forebrain white matter volume was decreased in APP48 mice as seen morphologically in the central white matter and the corpus callosum (***B***, stars) and as documented by quantitative assessment (Student's *t* test, two-tailed, $^{**}p < 0.01$; ***C***). ***D***, ***E***, The spinal cord was also ~10% smaller in APP48 mice (***E***) than in wild-type mice (***D***). However, morphological changes and especially white matter loss did not become obvious.

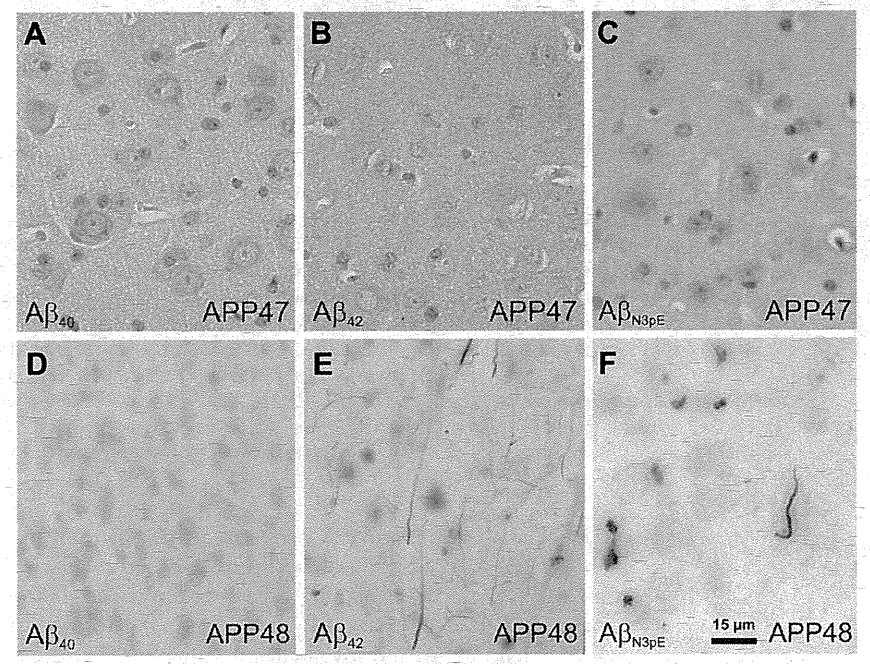

Figure 5. N3pEAβ staining in APP47 and APP48 mice. Neocortical sections from 18-month-old APP47 (***A–C***) and APP48 (***D***, ***E***) mice were immunostained with antibodies specific for $A\beta_{40}$ (***A***, ***D***), $A\beta_{42}$ (***B***, ***E***), or N3pEAβ (***C***, ***F***). As expected, APP47 brains were stained with $A\beta_{40}$ but not $A\beta_{42}$ antibodies, whereas APP48 reacted with $A\beta_{42}$ but not $A\beta_{40}$ antibodies. Pyroglutamate was found in neuropil Aβ grains and few dendritic Aβ treads but not in somatic Aβ granules of APP48 but not in APP47 mice. Scale bar, 15 μm.

after prolonged exposure was a band detectable in 21-month-old APP47 × APP48 mouse brains but not young double transgenic or the single-transgenic brains. In contrast, Aβ antibody 6E10 recognized the lower band to almost the same extent in young and old animals. Sequential immunoprecipitation with the N3pE followed by the 6E10 Aβ antibodies confirmed that only a minor Aβ fraction in this band contained pyroglutamate (data not shown). The main portion of the lowest band most likely corresponded to $A\beta_{4-40/42}$ in agreement with the lack of detection by antibody β1 against the $A\beta_{3-6}$ epitope (data not shown).

Age-related increase of insoluble $A\beta_{42}$ but not $A\beta_{40}$

To estimate the overall changes with age, total $A\beta_{42}$ in APP48 mice was analyzed after formic acid extraction of the cerebral cortex. An approximately threefold increase was found between 1 and 19 months of age (Fig. 3*A*). By contrast, $A\beta_{40}$ in APP47 mice remained at a similar level during aging (Fig. 3*B*). In aged double-transgenic APP47 × APP48 mice, $A\beta_{40}$ increased considerably compared with APP47 alone, while $A\beta_{42}$ reached the same level as found in APP48 (Fig. 3*C*).

These results and the discrepancy between mRNA and protein steady-state levels of $A\beta_{40}$ and $A\beta_{42}$ prompted us to analyze their solubility. Whereas Triton X-100 extraction almost completely solubilized $A\beta_{40}$ from APP47 brains, $A\beta_{42}$ in APP48 brain remained largely in the insoluble pellet after Triton X-100 and SDS extraction (data not shown). For more systematic analysis, forebrains from young and aged animals (1.5 and 21 months of age) were sequentially extracted with Triton X-100, SDS, and formic acid and analyzed by Western blotting (Fig. 3*D*). Regardless of the age, the initial Triton X-100 treatment completely extracted $A\beta_{40}$ from APP47 brain. In contrast, Triton X-100 hardly dissolved any $A\beta_{42}$ either from young or aged APP48 brains. $A\beta_{42}$ mostly distributed between the SDS and formic acid extracts. This is consistent with the very low level of $A\beta_{42}$ secretion from cells transfected with the same construct. Young APP47 × APP48 mice showed increased Aβ about equally distributed between the Triton X-100- and SDS-soluble fractions. Aβ in the SDS-insoluble material was hardly detectable. It increased considerably in this and the SDS fraction at old age, while the Triton X-100-soluble Aβ remained constant or decreased slightly. The complete extraction of the Aβ peptides in every step required large buffer

volumes and 2% SDS/sonication in the second step. Smaller extraction volumes or less harsh SDS treatment reduced the Aβ peptides in the corresponding fractions with a concomitant increase in the following extracts (data not shown). Independent of the extraction conditions, these data demonstrate an age-related increase of insoluble $A\beta_{42}$. Such an increase did not occur with $A\beta_{40}$ alone but was detectable in the presence of $A\beta_{42}$ (Fig. 3*D*). Aβ from a young APP23 transgenic mouse (APP with Swedish mutation) analyzed in parallel distributed between all fractions.

Distinct neuropathology after intracellular $A\beta_{42}$ expression

The forebrain weights of the different mouse lines were compared at 2 and 21 months of age. No significant difference from wild-type mice was found for APP47. However, APP48 mice showed a reduction in forebrain weight at 2 months, which became more pronounced with age. The same reduction was observed for double-transgenic mice of the corresponding age groups (Table 1). Further investigation of APP48 mice showed a reduced bihemispheric diameter in forebrain compared with wild-type animals (Fig. 4*A*,*B*). Quantitative analysis demonstrated a ~37% reduction in white matter volume (Fig. 4*C*). A slightly reduced overall size (~10%) was observed for the spinal cord (Fig. 4*D*,*E*) without other obvious changes.

Analyses of APP47 brains by Aβ immunohistochemistry demonstrated weak staining of $A\beta_{40}$ granules in the soma of neurons (Fig. 5*A*–*C*). N3pEAβ (pyroglutamate-Aβ) was not detected. Amyloid plaques or other signs of histopathology were not found even at the oldest age analyzed (24 months).

Immunohistochemistry did not detect amyloid plaques in APP48 mice even at the age of 24 months. Instead, three types of lesions were stained with different Aβ antibodies (MBC42, 4G8, NT11, AβN1D): (1) dendrites filled with Aβ-positive material of thread-like appearance (dendritic Aβ threads), (2) dot-like granules in the soma of nerve cells (somatic Aβ granules), and (3) grain-like structures in the neuropil (Aβ grains) (Figs. 5*E*, 6*A*–*G*). The three types of Aβ lesions were found throughout the entire gray matter of the CNS. Their distribution varied among different CNS regions with the most severe pathology in neocortical and allocortical areas (Table 2). Aβ threads were less frequently found in the brainstem and cerebellum and were not seen in the spinal cord, whereas Aβ granules were found in all these regions (Fig. 6*I*,*J*). Staining with an N3pEAβ antibody visualized Aβ grains, few dendritic Aβ threads, but no somatic Aβ granules (Fig. 5*E*,*F*). Aβ-positive lesions in APP48 mice were not stained with an $A\beta_{40}$ antibody (Fig. 5*D*).

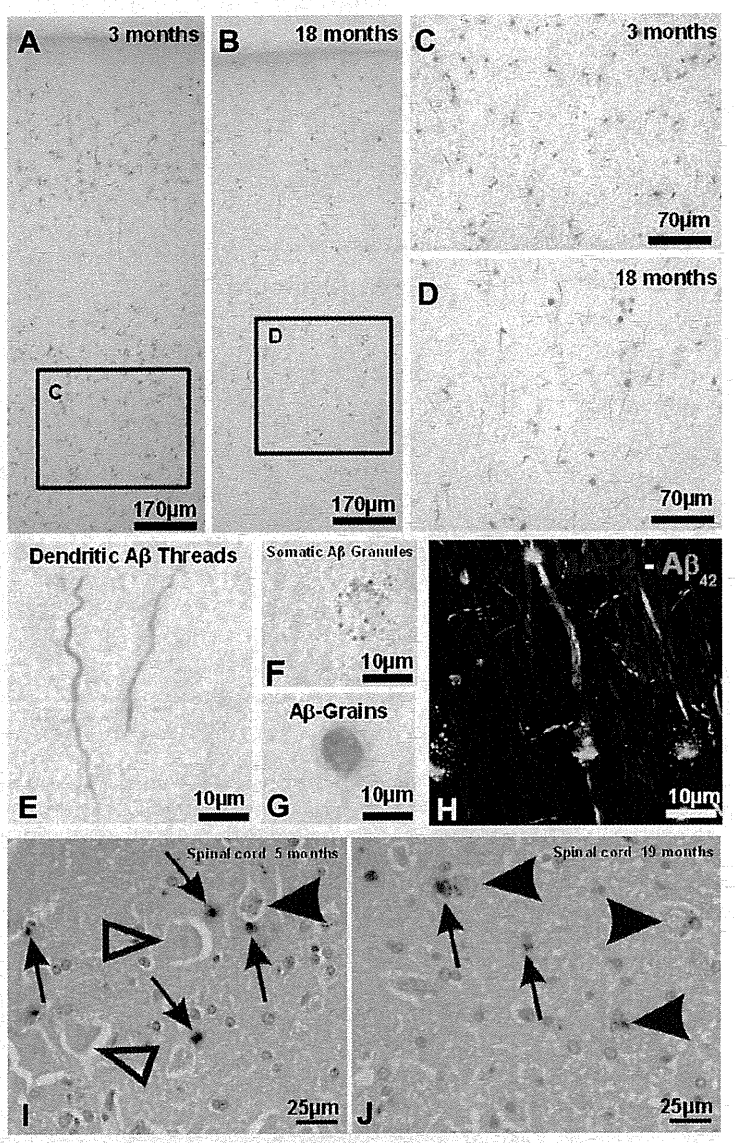

Figure 6. Aβ lesions in APP48 mice. ***A***, ***B***, In the neocortex, Aβ changes were mainly located in layers II, III, V, and VI in 3- as well as in 18-month-old animals. No amyloid plaques were visible. ***C***, At 3 months of age, Aβ antibodies predominantly stained grain-like structures, whereas thread-like material and somatic granules were less frequently found. ***D***, In 18-month-old APP48 mice, thread-like lesions predominated, while grains and granules became less abundant (see Fig. 8 for quantification). ***E–G***, Higher magnification of the three major Aβ accumulations in APP48 mice: dendritic Aβ threads (***E***) representing dendrites filled with Aβ; somatic Aβ granules (***F***), which are dot-like Aβ-positive structures within the perikaryon of neurons. They were distributed in the cell soma; Aβ grains (***G***) representing extraneuronal accumulations of Aβ. ***H***, Double-label immunofluorescence for Aβ and MAP2 confirmed the dendritic localization of the Aβ threads. These three Aβ lesions are found throughout the gray matter of the CNS, although Aβ threads were missing in the spinal cord (***I***, ***J***). ***I***, At 5 months of age, Aβ grains were predominant (arrows). Only few interneurons with somatic granules were observed (black arrowhead). Motor neurons were free of Aβ (open arrowheads). ***J***, At 19 months of age, somatic granules were also seen in motor neurons (arrowheads) and Aβ grains were less abundant (arrows).

Double-label immunohistochemistry corroborated the presence of Aβ in MAP2-positive dendrites of APP48 mice (Fig. 6*H*). Campbell–Switzer silver staining indicated a fibrillar structure of dendritic Aβ with the pattern of threads (Fig. 7*A*). Ultrastructurally, the dendritic Aβ-positive material showed a fibril-like appearance (Fig. 7*B*,*C*). Axonal Aβ was not observed. The intracellular location of somatic Aβ granules was further analyzed by immuno-electron microscopy, which detected Aβ-positive material in lysosomes of neurons (Fig. 7*D*,*E*). Neuropil grains were associated with CD45-positive microglial cells (Fig.

Table 2. Distribution of morphological changes in APP48 mice

Brain regions	Conventional histology	$A\beta_{42}$ staining
Neocortex	—	Aβ grains, Aβ granules, Aβ threads
Allocortex (including hippocampus)	Reduction of neurons in CA1	Few Aβ grains, Aβ granules, Aβ threads
Basal ganglia	—	Aβ grains, Aβ threads
Thalamus	—	Aβ grains, Aβ granules, and few Aβ threads
Basal forebrain nuclei	—	Aβ granules, single Aβ threads, and Aβ grains in aged animals
Midbrain	—	Aβ granules, single Aβ threads, and Aβ grains in aged animals
Brainstem	—	Aβ granules, single Aβ threads, and Aβ grains in aged animals
Cerebellum: dentate nucleus	—	Aβ granules, single Aβ threads, and Aβ grains in aged animals
Cerebellum: granule cell layer	—	Aβ grains
Cerebellum: Purkinje cells	—	—
Spinal cord	Reduction of spinal cord diameter	Aβ grains, Aβ granules
Cerebral, cerebellar, and spinal white matter	Reduction of cerebral white matter in aged animals	—

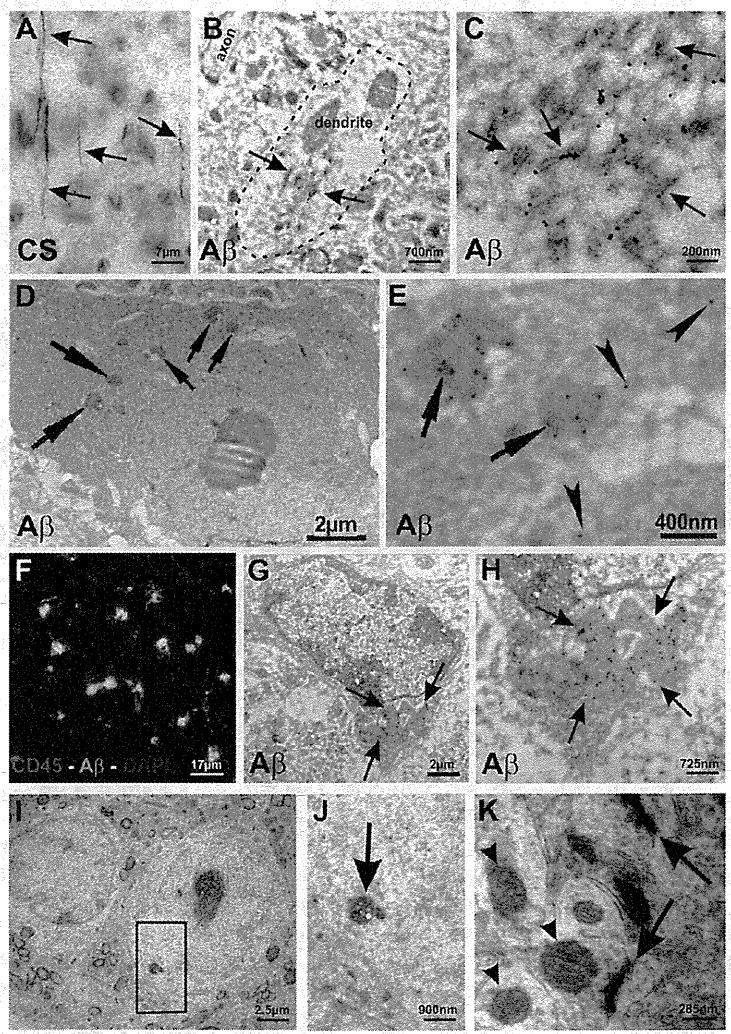

Figure 7. Immuno-electron-microscopic localization of Aβ lesions and ultrastructural analyzes. ***A***, Campbell–Switzer silver staining of dendritic Aβ threads indicated the fibrillar nature of the aggregates (arrows). ***B***, At the immuno-electron-microscopic level, a distinct number of dendrites (example marked by the dashed line) in the neuropil of the frontocentral neocortex contained Aβ-positive material (arrows). Note that the axon did not contain Aβ. ***C***, At higher magnification, the Aβ-positive dendritic material exhibited a fibrillar structure (arrows) consistent with the SDS resistance of an $A\beta_{1-42}$ subpopulation. ***D***, Immuno-electron microscopy showed a neuron with somatic Aβ granules. ***E***, Higher magnification (area of the top two arrows in ***D***) detected Aβ within lysosomes (arrows) and more rarely in the endoplasmic reticulum (arrowheads). ***F***, Double-label immunofluorescence indicated that Aβ grains (labeled in green) were associated with CD45-positive microglial cells. ***G***, Using immuno-electron microscopy, microglial cells were found, which exhibited lysosomal $A\beta_{42}$-reactive material. ***H***, Higher magnification of the lysosomal region outlined by arrows. ***I–K***, Epon-embedded tissue exhibited a better structural resolution than the immuno-electron material. ***I***, Neurons did not show obvious alterations of their subcellular organization. ***J***, No specific changes were found in lysosomes (arrow) at higher magnification (***I***, frame). ***K***, Dendrites and synapses appeared normal. Mitochondria (arrowheads) within the dendrites and axons showed no obvious changes (arrows indicate dendritic threads).

7*F*). Immuno-electron microscopy confirmed the microglial Aβ inclusions and indicated a lysosomal association (Fig. 7*G*,*H*). We did not observe Aβ in multivesicular bodies of APP48 mice but found minor staining in the endoplasmic reticulum (Fig. 7*E*, arrowheads).

Double-labeling immunofluorescence showed colocalization of neuronal Aβ granules and microglial Aβ grains with BIP and LAMP-1 in agreement with a late endosomal/lysosomal localization of both structures (Fig. 8*A–I*). Dendritic Aβ threads did not colocalize with BIP and LAMP-1, further indicating that these aggregates are different from Aβ granules and grains (Fig. 8*J–L*). No colocalization was found with markers for early endosomes (EEA1) and stress granules [TIA/TIAR(D-9)] (data not shown).

Structural analysis in Epon-embedded sections by electron microscopy revealed few lysosomal, lipofuscin-like aggregates in the soma of neurons (Fig. 7*I*,*J*). Further structural changes, especially in dendrites, were neither detected at the ultrastructural (Fig. 7*K*) nor at the light-microscopic level. Immunohistochemisty did not show alterations of the dendritic tree or of axons in neurofilament-stained sections of 3- and 18-month-old APP48 mice when comparing with age-matched wild-type animals. Dystrophic neurites were not observed in the APP staining. The cortical distribution of synaptophysin-positive material did not differ between APP48 and wild-type mice. Abnormally phosphorylated tau and pTDP-43 were not found in the brains of APP48 mice. There were no obvious differences in the distribution pattern of GFAP-positive astrocytes and RCA-positive microglial cells between wild-type and APP48 mice. APP47 × APP48 mice showed qualitatively similar alterations as APP48.

Quantification of the three Aβ lesions in the frontocentral cortex of APP48 mice (Fig. 9*A–C*) revealed an approximately

threefold increase in the number of dendritic Aβ threads between 3 and 18 month of age. In contrast, an age-dependent ~45–48% decrease of Aβ granules and grains was found. The frontocentral neocortex did not show alterations in neuron number compared with wild-type mice (Fig. 9*D*). However, we found considerable neuron loss in the hippocampus at 3 and 18 months of age (Fig. 9*E*).

Motor deficit in APP48 mice

Compared with wild-type animals the APP47 genotype had no significant effect on body weight, while it was reduced in APP48 at 12 to 15 months (Table 3). Inspection over time showed no difference from wild type at 1 month but a body weight reduction from 2 months onward. An intermediate weight was found for double-transgenic APP47 × APP48 mice. APP48 but not APP47 mice presented with minor motor anomalies at ~6 months, which increased with age, and occasionally paralysis developed above 18 months of age. No increase in spontaneous mortality was apparent in these mouse lines.

To evaluate the apparent motor deficit quantitatively, 5- to 7-month-old APP48 were analyzed in the Rotarod test compared with littermate controls (Fig. 10). During three consecutive trials done, APP48 mice fell off the rod much more quickly than the controls. These data indicate a considerable impairment in motor coordination in aged APP48 mice.

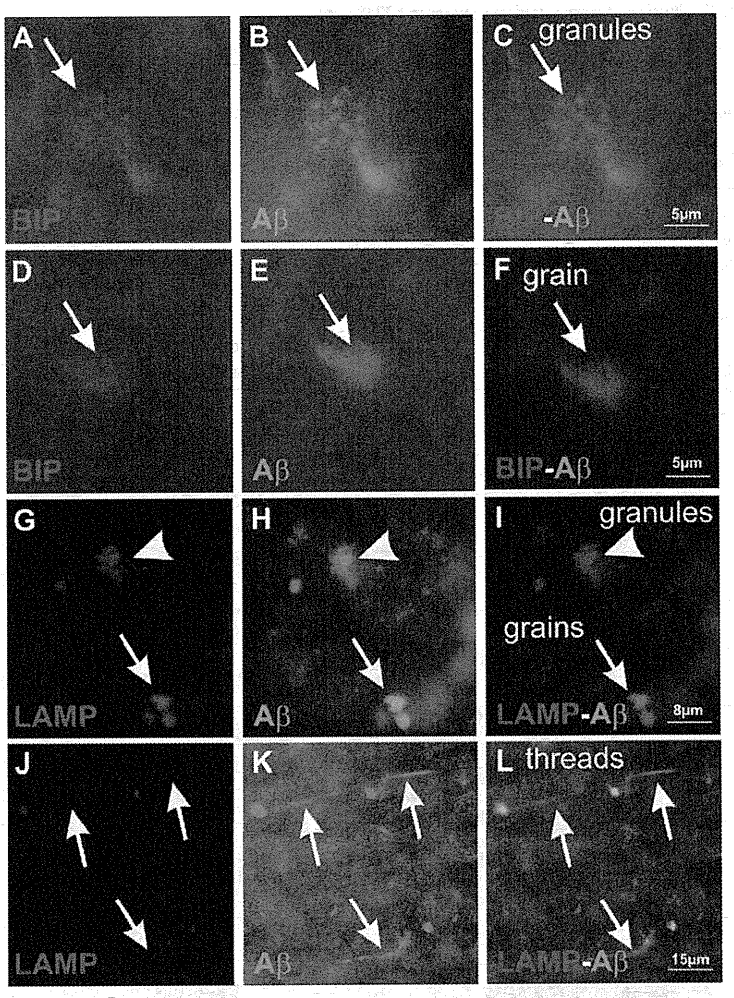

Figure 8. Localization of Aβ lesions at intracellular membrane compartments by double immunolabeling. Double-label immunohistochemistry for BIP (***A***, ***D***), a marker of post-endoplasmatic reticulum compartments, and Aβ (***B***, ***E***) showed colocalization of BIP and Aβ (***C***, ***F***) in Aβ granules (***A–C***, arrow) and microglial Aβ grains (***D–F***, arrow). The lysosomal marker LAMP-1 (***G***) demonstrated a similar colocalization (***I***) with Aβ (***H***) in granules (arrowhead) and grains (arrow) as BIP, indicating their lysosomal location. Aβ labeling (***K***) of dendritic threads (***J–L***, arrows) did not colocalize (***L***) with the lysosomal marker LAMP-1 (***J***), further distinguishing Aβ threads from Aβ granules and grains.

Discussion

In the present study, we describe transgenic mouse lines expressing $A\beta_{1-40}$ (APP47) and $A\beta_{1-42}$ (APP48) in neurons. The expression constructs encode a signal sequence to insert both Aβ peptides into the endoplasmic reticulum presumably with a similar orientation as after cleavage from APP. In contrast to regular cleavage of Aβ from APP, which largely occurs in endosomes and is followed by rapid secretion (Selkoe et al., 1996), the Aβ peptides are synthesized in the endoplasmic reticulum. Cell culture studies have shown substantial amounts of intracellular Aβ and comparably little secretion in particular of $A\beta_{1-42}$ (Maruyama et al., 1995) (our unpublished data).

Brains from young APP48 mice contained considerably more Aβ than the corresponding APP47 brains, while the inverse was true on the mRNA level. Different translational efficacies of these very similar constructs appear unlikely. Moreover, the mRNA levels remained unchanged in APP47 × APP48 mice relative to the parent lines, whereas the amount of both Aβ isoforms was considerably altered. This argues in favor of a differential post-translational regulation of the Aβ isoforms. A higher clearance of $A\beta_{1-40}$ has been observed after brain injection (Ji et al., 2001), and this more soluble peptide may also undergo faster intracellular degradation. Accordingly, $A\beta_{1-40}$ in APP47 mice remained at a similar level during aging, whereas $A\beta_{1-42}$ showed a moderate elevation in APP48 mice.

$A\beta_{1-42}$ seems able to stabilize $A\beta_{1-40}$ albeit at the expense of its own stability. In young APP47 × APP48 mice, $A\beta_{1-42}$ was decreased and more soluble while $A\beta_{1-40}$ was increased compared with the parent lines. The relative ratio of both peptides may strongly influence their stability as indicated by a recent *in vitro* study (Kuperstein et al., 2010). During aging of APP47 × APP48 mice, $A\beta_{1-42}$ increased moderately just compensating the decrease at young age compared with the single-transgenic mice (APP48). For $A\beta_{1-40}$, a very large increase was found in double- compared with single-transgenic mice (APP47). Consistent with an intracellular interaction of both Aβ peptides, no such effect on the steady-state levels was observed when both peptides were fused to the C terminus of the BRI protein and rapidly secreted after cleavage (Kim et al., 2007). However, intracellular Aβ cannot be completely excluded in these mice as its analysis has not been a topic of the study. Nonetheless, secreted $A\beta_{1-40}$ inhibited amyloid deposition in APP transgenic mice, which indicates an extracellular interaction affecting overall solubility of the Aβ peptides.

Among the lines, APP48 mice develop the more advanced pathology and show three types of Aβ lesions. Neurons contain

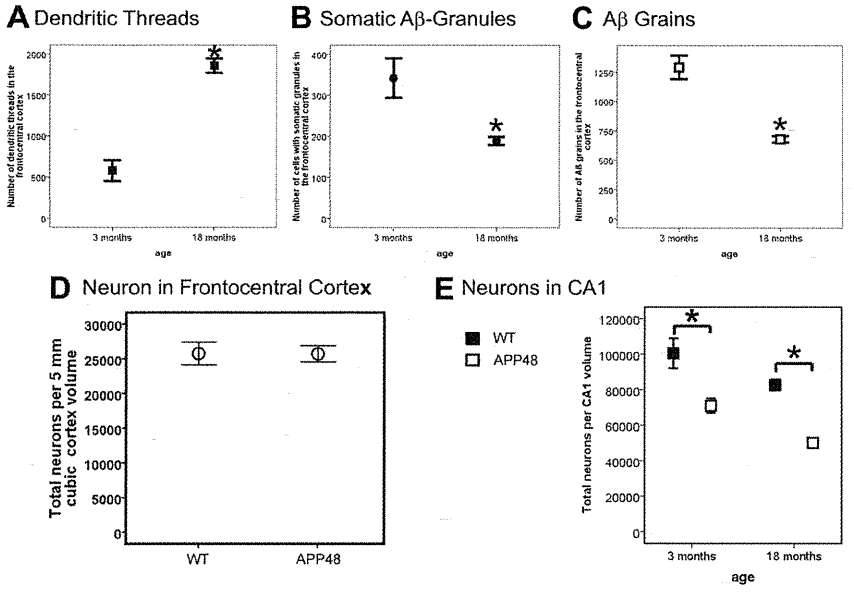

Figure 9. Quantification of Aβ lesions and neuron numbers in APP48 mice. Dendritic Aβ threads (***A***), somatic Aβ granules (***B***), and microglia Aβ grains (***C***) were quantified in the frontocentral neocortex of 3- and 18-month-old APP48 mice. This analysis revealed an increase in the number of dendritic Aβ threads with age but a decrease of somatic Aβ granules and microglial Aβ grains. Stereology was used to quantify neurons in the frontal cortex (***D***) of 18-month-old APP48 mice compared with wild-type littermate controls, which did not show a difference ($p = 0.613$). The total number of neurons was reduced in hippocampus (***E***) at both 3 and 18 months of age. Significant differences are indicated (Student's *t* test, two-tailed, $*p < 0.05$).

Table 3. Average body weight of APP47, APP48, and double-transgenic mice at 12–15 months of age

Gender	Body weight	Wild type	APP47	APP48	APP47 × APP48
Females	Body weight (g)[a]	39 ± 5	38 ± 5	23 ± 3	30 ± 5
	p (vs wild type)*		NS	<0.0001	<0.0001
Males	Body weight (g)[a]	45 ± 10	41 ± 6	30 ± 4	36 ± 5
	p (vs wild type)*		NS	<0.0001	<0.005

[a]Shown are mean ± SD.

*Student's *t* test, two-tailed. NS, Nonsignificant.

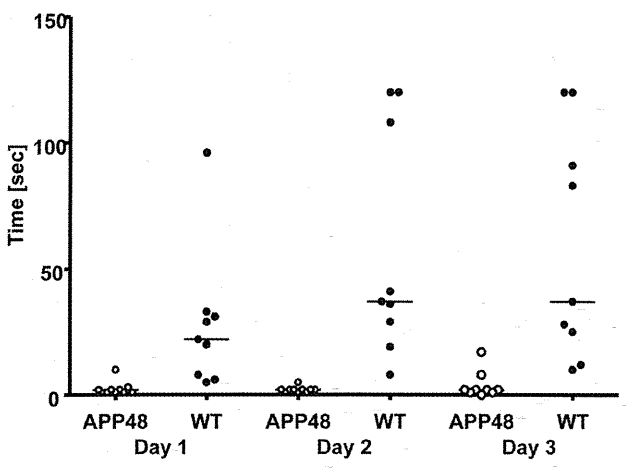

Figure 10. Motor impairment of APP48 mice. APP48 mice (open circles) and littermate controls (closed circles) at the age of 5–7 months were evaluated in the Rotarod test on 3 consecutive days. The time on the rod is shown for each individual animal, and the median is indicated. In all three tests, APP48 mice stayed significantly less long on the rod than the controls (Mann–Whitney *U* test; trial 1, $p < 0.001$; trial 2, $p < 0.0003$; trial 3, $p < 0.0007$).

Aβ threads in dendrites and somatic Aβ granules in lysosomes. Additionally, Aβ grains are present in lysosomes of microglia cells. Dendritic Aβ threads appear fibrillar at the electron-microscopic level and can be silver stained. They accumulate with age possibly because their fibrillar structure prevents efficient degradation. In contrast, $A\beta_{1-42}$ found as granules in neuronal lysosomes neither appears fibrillar nor shows other evidence of accumulation, suggesting that it may be degraded. With progressing dendritic Aβ aggregation, an increased number of assembly sites becomes available. These changes may lead to a shift of Aβ toward dendritic threads and a reduced lysosomal transport resulting in the observed decrease of Aβ granules with age. The detection of Aβ in dendrites and lysosomes demonstrates that the peptide is transported within the neuron from the site of synthesis at the endoplasmic reticulum to other locations. The small Aβ signal in the endoplasmic reticulum observed at the electron-microscopic level is in agreement with the synthesis of Aβ at this location. We did not detect Aβ in multivesicular bodies as described for APP transgenic mice and AD brain (Takahashi et al., 2002). APP47 mice only show somatic Aβ granules consistent with a more rapid and complete degradation of $A\beta_{1-40}$.

In APP48 brain, Aβ is also found in microglial lysosomes even though the Thy-1 cassette drives expression in neurons (Calhoun et al., 1999). It may derive from Aβ secretion known to occur to a certain extent in cell culture. Alternatively, microglial Aβ may originate from degenerated neurons or neuronal processes, but the lack of PAS-positive lysosomal/lipofuscin-like material and the absence of phagosomes at the electron-microscopic level argue against strong phagocytosis. Interestingly, the very small amount of pyroglutamate Aβ is mainly associated with microglial but not neuronal lysosomes, indicating that pyroglutamate-Aβ (N3pEAβ) formation is largely avoided when Aβ is directly targeted for degradation. In agreement with a slow conversion of $A\beta_{1-42}$ to pyroglutamate Aβ, this isoform was also detected in dendritic threads.

Intracellular Aβ in APP47 and APP48 mice does not lead to amyloid plaque formation, although the total brain Aβ concentrations are comparable with preplaque APP transgenic mice, which form plaques during aging (Abramowski et al., 2008). Intracellular membrane expression and aggregation of Aβ as in APP48 is apparently not sufficient for plaque formation. This does not exclude that plaque development requires Aβ generation and aggregation in a specific intracellular location, which is reached by APP or its C-terminal fragments but not by Aβ as it lacks the trafficking signals. However, intraneuronal Aβ accumulation in the absence of extracellular amyloid plaques has also been observed in transgenic mice expressing APP with the AD-linked E693Δ mutation (Tomiyama et al., 2010). In contrast, amyloid plaque formation has been observed in $A\beta_{1-42}$ transgenic mice using the BRI protein as vehicle to secrete the Aβ peptides (McGowan et al., 2005). Together, the studies favor the notion that amyloid plaques are formed after secretion of Aβ. Single diffuse plaques have also been observed in $A\beta_{3-42}$ trans-

genic mice, which produce considerable N3pEAβ (Wirths et al., 2009). The strong tendency of N3pEAβ to aggregate (Schlenzig et al., 2009) in combination with a low level of secretion may be sufficient for plaque formation.

We did not observe further structural changes associated with dendritic Aβ threads and lysosomal granules or grains. It is possible that dendritic threads or potential related soluble Aβ aggregates impair neuronal function in the absence of further structural changes. The pathological significance of increased lysosomal Aβ in granules and grains is less clear, and their reduction during aging argues against a role in degeneration or functional impairment. APP48 mice show a dramatically reduced neuron number in hippocampus, but no such change was detectable in frontal cortex. A similar discrepancy has been found in APP23 mice (Calhoun et al., 1998) and may be related to the higher vulnerability of hippocampal neurons. Additionally, APP48 mice loose brain weight, apparently due to a severe white matter reduction. These findings suggest a loss of myelinated axons in the absence of extensive pathology as observed in AD and other neurodegenerative diseases (Ihara et al., 2010). The white matter atrophy may be mainly explained by the severe hippocampal neuron loss. These neurons project to other cortical areas constituting a significant number of axons in the white matter. No obvious loss of neurons involved in motor function and coordination was found, which would explain the motor deficits observed in APP48. However, degeneration of axons from such neurons or their functional impairment appears possible in view of the fibrillar Aβ thread pathology in neurons relevant for motor function and coordination (motor cortex, basal ganglia, and cerebellar dentate nucleus). A primary alteration of spinal motor neurons seems less likely because skeletal muscles did not exhibit the pattern of spinal muscular atrophy.

Hippocampal neuron loss is already present at 3 months of age and does not progress much further. It appears that most of the detectable toxicity of intracellular Aβ occurs shortly after postnatal onset of strong Thy-1 promoter expression. Compared with APP transgenic mice, APP48 develop an overlapping but distinct pathology. None of these models including BRI-Aβ mice (McGowan et al., 2005) develops most of the non-Aβ pathology typical of AD. In all systems including AD brain, Aβ aggregates do not show strong acute toxicity but may lead to a slow deregulation of neuronal networks (Palop and Mucke, 2010). The APP48 animal model described here indicates that $A\beta_{1-42}$ generated at the luminal membrane side can form intracellular Aβ aggregates and induce some neurodegeneration, most notably in hippocampus, white matter atrophy, and motor deficits.

References

Abramowski D, Wiederhold KH, Furrer U, Jaton AL, Neuenschwander A, Runser MJ, Danner S, Reichwald J, Ammaturo D, Staab D, Stoeckli M, Rueeger H, Neumann U, Staufenbiel M (2008) Dynamics of A beta turnover and deposition in different beta-amyloid precursor protein transgenic mouse models following gamma-secretase inhibition. J Pharmacol Exp Ther 327:411–424.

Braak H (1974) On the structure of the human archicortex. I. The cornu ammonis. A Golgi and pigmentarchitectonic study. Cell Tissue Res 152:349–383.

Braak H, Braak E (1991) Demonstration of amyloid deposits and neurofibrillary changes in whole brain sections. Brain Pathol 1:213–216.

Calhoun ME, Wiederhold KH, Abramowski D, Phinney AL, Probst A, Sturchler-Pierrat C, Staufenbiel M, Sommer B, Jucker M (1998) Neuron loss in APP transgenic mice. Nature 395:755–756.

Calhoun ME, Burgermeister P, Phinney AL, Stalder M, Tolnay M, Wiederhold KH, Abramowski D, Sturchler-Pierrat C, Sommer B, Staufenbiel M, Jucker M (1999) Neuronal overexpression of mutant amyloid precursor protein results in prominent deposition of cerebrovascular amyloid. Proc Natl Acad Sci U S A 96:14088–14093.

Capetillo-Zarate E, Staufenbiel M, Abramowski D, Haass C, Escher A, Stadelmann C, Yamaguchi H, Wiestler OD, Thal DR (2006) Selective vulnerability of different types of commissural neurons for amyloid β-protein-induced neurodegeneration in APP23 mice correlates with dendritic tree morphology. Brain 129:2992–3005.

Citron M (2010) Alzheimer's disease: strategies for disease modification. Nat Rev Drug Discov 9:387–398.

Gouras GK, Tampellini D, Takahashi RH, Capetillo-Zarate E (2010) Intraneuronal beta-amyloid accumulation and synapse pathology in Alzheimer's disease. Acta Neuropathol 119:523–541.

Hsu SM, Raine L, Fanger H (1981) Use of avidin-biotin-peroxidase complex (ABC) in immunoperoxidase techniques: a comparison between ABC and unlabeled antibody (PAP) procedures. J Histochem Cytochem 29:577–580.

Ihara M, Polvikoski TM, Hall R, Slade JY, Perry RH, Oakley AE, Englund E, O'Brien JT, Ince PG, Kalaria RN (2010) Quantification of myelin loss in frontal lobe white matter in vascular dementia, Alzheimer's disease, and dementia with Lewy bodies. Acta Neuropathol 119:579–589.

Jack CR Jr, Knopman DS, Jagust WJ, Shaw LM, Aisen PS, Weiner MW, Petersen RC, Trojanowski JQ (2010) Hypothetical model of dynamic biomarkers of the Alzheimer's pathological cascade. Lancet Neurol 9:119–128.

Ji Y, Permanne B, Sigurdsson EM, Holtzman DM, Wisniewski T (2001) Amyloid beta40/42 clearance across the blood-brain barrier following intra-ventricular injections in wild-type, apoE knock-out and human apoE3 or E4 expressing transgenic mice. J Alzheimers Dis 3:23–30.

Kang J, Lemaire HG, Unterbeck A, Salbaum JM, Masters CL, Grzeschik KH, Multhaup G, Beyreuther K, Müller-Hill B (1987) The precursor of Alzheimer's disease amyloid A4 protein resembles a cell-surface receptor. Nature 325:733–736.

Kim J, Onstead L, Randle S, Price R, Smithson L, Zwizinski C, Dickson DW, Golde T, McGowan E (2007) Aβ40 inhibits amyloid deposition *in vivo*. J Neurosci 27:627–633.

Klafki HW, Wiltfang J, Staufenbiel M (1996) Electrophoretic separation of betaA4 peptides (1–40) and (1–42). Anal Biochem 237:24–29.

Kuperstein I, Broersen K, Benilova I, Rozenski J, Jonckheere W, Debulpaep M, Vandersteen A, Segers-Nolten I, Van Der Werf K, Subramaniam V, Braeken D, Callewaert G, Bartic C, D'Hooge R, Martins IC, Rousseau F, Schymkowitz J, De Strooper B (2010) Neurotoxicity of Alzheimer's disease Abeta peptides is induced by small changes in the Abeta42 to Abeta40 ratio. EMBO J 29:3408–3420.

Lüthi A, Van der Putten H, Botteri FM, Mansuy IM, Meins M, Frey U, Sansig G, Portet C, Schmutz M, Schröder M, Nitsch C, Laurent JP, Monard D (1997) Endogenous serine protease inhibitor modulates epileptic activity and hippocampal long-term potentiation. J Neurosci 17:4688–4699.

Maruyama K, Tagawa K, Kawamura Y, Asada H, Ishiura S, Obata K (1995) Secretion of Alzheimer beta/A4 protein (1–40) and intracellular retention of beta/A4 protein (1–42) in transfected COS cells. Biochem Biophys Res Commun 207:971–977.

McGowan E, Pickford F, Kim J, Onstead L, Eriksen J, Yu C, Skipper L, Murphy MP, Beard J, Das P, Jansen K, Delucia M, Lin WL, Dolios G, Wang R, Eckman CB, Dickson DW, Hutton M, Hardy J, Golde T (2005) Abeta42 is essential for parenchymal and vascular amyloid deposition in mice. Neuron 47:191–199.

Nimmrich V, Ebert U (2009) Is Alzheimer's disease a result of presynaptic failure? Synaptic dysfunctions induced by oligomeric beta-amyloid. Rev Neurosci 20:1–12.

Palop JJ, Mucke L (2010) Amyloid-beta-induced neuronal dysfunction in Alzheimer's disease: from synapses toward neural networks. Nat Neurosci 13:812–818.

Reichwald J, Danner S, Wiederhold KH, Staufenbiel M (2009) Expression of complement system components during aging and amyloid deposition in APP transgenic mice. J Neuroinflammation 6:35.

Saido TC, Iwatsubo T, Mann DM, Shimada H, Ihara Y, Kawashima S (1995) Dominant and differential deposition of distinct beta-amyloid peptide species, A beta N3(pE), in senile plaques. Neuron 14:457–466.

Schlenzig D, Manhart S, Cinar Y, Kleinschmidt M, Hause G, Willbold D, Funke SA, Schilling S, Demuth HU (2009) Pyroglutamate formation influences solubility and amyloidogenicity of amyloid peptides. Biochemistry 48:7072–7078.

Schmitz C, Hof PR (2000) Recommendations for straightforward and rig-

orous methods of counting neurons based on a computer simulation approach. J Chem Neuroanat 20:93–114.

Selkoe DJ, Yamazaki T, Citron M, Podlisny MB, Koo EH, Teplow DB, Haass C (1996) The role of APP processing and trafficking pathways in the formation of amyloid beta-protein. Ann N Y Acad Sci 777:57–64.

Shankar GM, Li S, Mehta TH, Garcia-Munoz A, Shepardson NE, Smith I, Brett FM, Farrell MA, Rowan MJ, Lemere CA, Regan CM, Walsh DM, Sabatini BL, Selkoe DJ (2008) Amyloid-beta protein dimers isolated directly from Alzheimer's brains impair synaptic plasticity and memory. Nat Med 14:837–842.

Staufenbiel M, Paganetti PA (2000) Electrophoretic separation and immunoblotting of $A\beta1-40$ and $A\beta1-42$. Methods Mol Med 32:91–99.

Sturchler-Pierrat C, Abramowski D, Duke M, Wiederhold KH, Mistl C, Rothacher S, Ledermann B, Bürki K, Frey P, Paganetti PA, Waridel C, Calhoun ME, Jucker M, Probst A, Staufenbiel M, Sommer B (1997) Two amyloid precursor protein transgenic mouse models with Alzheimer disease-like pathology. Proc Natl Acad Sci U S A 94:13287–13292.

Takahashi RH, Milner TA, Li F, Nam EE, Edgar MA, Yamaguchi H, Beal MF, Xu H, Greengard P, Gouras GK (2002) Intraneuronal Alzheimer abeta42 accumulates in multivesicular bodies and is associated with synaptic pathology. Am J Pathol 161:1869–1879.

Thal DR, Sassin I, Schultz C, Haass C, Braak E, Braak H (1999) Fleecy amyloid deposits in the internal layers of the human entorhinal cortex are comprised of N-terminal truncated fragments of Abeta. J Neuropathol Exp Neurol 58:210–216.

Thal DR, Larionov S, Abramowski D, Wiederhold KH, Van Dooren T, Yamaguchi H, Haass C, Van Leuven F, Staufenbiel M, Capetillo-Zarate E (2007) Occurrence and co-localization of amyloid beta-protein and apolipoprotein E in perivascular drainage channels of wild-type and APP-transgenic mice. Neurobiol Aging 28:1221–1230.

Tomiyama T, Matsuyama S, Iso H, Umeda T, Takuma H, Ohnishi K, Ishibashi K, Teraoka R, Sakama N, Yamashita T, Nishitsuji K, Ito K, Shimada H, Lambert MP, Klein WL, Mori H (2010) A mouse model of amyloid β oligomers: their contribution to synaptic alteration, abnormal tau phosphorylation, glial activation, and neuronal loss *in vivo*. J Neurosci 30:4845–4856.

Wirths O, Breyhan H, Cynis H, Schilling S, Demuth HU, Bayer TA (2009) Intraneuronal pyroglutamate-Abeta 3–42 triggers neurodegeneration and lethal neurological deficits in a transgenic mouse model. Acta Neuropathol 118:487–496.

Yamaguchi H, Sugihara S, Ogawa A, Saido TC, Ihara Y (1998) Diffuse plaques associated with astroglial amyloid beta protein, possibly showing a disappearing stage of senile plaques. Acta Neuropathol 95:217–222.

Journal of Cellular and Molecular Medicine
A JOURNAL OF TRANSLATIONAL MEDICINE

J. Cell. Mol. Med. Vol 16, No 2, 2012 pp. 287-295

High-molecular weight Aβ oligomers and protofibrils are the predominant Aβ species in the native soluble protein fraction of the AD brain

Ajeet Rijal Upadhaya [a], Irina Lungrin [a, b], Haruyasu Yamaguchi [c], Marcus Fändrich [d], Dietmar Rudolf Thal [a, *]

[a] *Laboratory of Neuropathology-Institute of Pathology, Center for Clinical Research at the University of Ulm, Ulm, Germany*
[b] *Department of Neurology, Center for Clinical Research at the University of Ulm, Ulm, Germany*
[c] *Gunma University of Health Sciences, Maebashi, Gunma, Japan*
[d] *Max Planck Research Unit for Enzymology of Protein Folding and Martin-Luther University Halle-Wittenberg, Halle an der Saale, Germany*

Received: November 3, 2010; Accepted: March 7, 2011

Abstract

Alzheimer's disease (AD) is characterized by the aggregation and deposition of amyloid β protein (Aβ) in the brain. Soluble Aβ oligomers are thought to be toxic. To investigate the predominant species of Aβ protein that may play a role in AD pathogenesis, we performed biochemical analysis of AD and control brains. Sucrose buffer-soluble brain lysates were characterized in native form using blue native (BN)-PAGE and also in denatured form using SDS-PAGE followed by Western blot analysis. BN-PAGE analysis revealed a high-molecular weight smear (>1000 kD) of $Aβ_{42}$-positive material in the AD brain, whereas low-molecular weight and monomeric Aβ species were not detected. SDS-PAGE analysis, on the other hand, allowed the detection of prominent Aβ monomer and dimer bands in AD cases but not in controls. Immunoelectron microscopy of immunoprecipitated oligomers and protofibrils/fibrils showed spherical and protofibrillar Aβ-positive material, thereby confirming the presence of high-molecular weight Aβ (hiMWAβ) aggregates in the AD brain. *In vitro* analysis of synthetic $Aβ_{40}$- and $Aβ_{42}$ preparations revealed Aβ fibrils, protofibrils, and hiMWAβ oligomers that were detectable at the electron microscopic level and after BN-PAGE. Further, BN-PAGE analysis exhibited a monomer band and less prominent low-molecular weight Aβ (loMWAβ) oligomers. In contrast, SDS-PAGE showed large amounts of loMWAβ but no $hiMWAβ_{40}$ and strikingly reduced levels of $hiMWAβ_{42}$. These results indicate that hiMWAβ aggregates, particularly $Aβ_{42}$ species, are most prevalent in the soluble fraction of the AD brain. Thus, soluble hiMWAβ aggregates may play an important role in the pathogenesis of AD either independently or as a reservoir for release of loMWAβ oligomers.

Keywords: amyloid β protein • protofibrils • fibrils • oligomers • Alzheimer's disease

Introduction

Alzheimer's disease (AD) is characterized by the extracellular deposition of amyloid β protein (Aβ) aggregates in the brain [1]. Although high-molecular weight Aβ (hiMWAβ) oligomers, Aβ protofibrils and fibrils, low-molecular weight Aβ (loMWAβ) oligomers, such as dimers, trimers or Aβ*56, have been observed in human AD brain tissue or in mouse models of AD [1–9], it is not entirely clear which Aβ species are the most relevant ones for the development of AD and how these Aβ forms are related to one another *in vivo*. Some studies have used SDS-PAGE for protein analysis [3–5, 9], which denatures and dissociates proteins into individual polypeptides before determining its molecular weight. By contrast, others have performed only dot blot analysis [6]. Currently, only size exclusion chromatography has been used to study oligomers in non-SDS-treated conditions [3, 9]. However, it

*Correspondence to: Dietmar R. THAL,
Laboratory of Neuropathology-Institute of Pathology,
Center for Clinical Research at the University of Ulm,
Helmholtzstrasse 8/1, D-89081 Ulm, Germany.
Tel.: +49-8221-96-2163
Fax: +49-8221-96-28158
E-mail: Dietmar.Thal@uni-ulm.de

doi:10.1111/j.1582-4934.2011.01306.x

is unclear whether interactions with the stationary phase may impact the aggregation state of hiMWAβ species. A detailed analysis of the native Aβ aggregates in the AD brain using blue native-PAGE (BN-PAGE) in comparison with SDS-PAGE analysis that focuses on the identification of the above-mentioned forms of Aβ aggregates is still unavailable.

Antibodies and antibody fragments have been developed to detect specific hiMWAβ oligomers (A11) and protofibrillar/fibrillar conformations (B10AP) [2, 6]. These antibodies and antibody fragments allow isolation of oligomers, protofibrils and fibrils from soluble native protein lysates by immunoprecipitation for further protein analysis. Here, we employed these antibodies and BN-PAGE analysis to clarify whether soluble hiMWAβ oligomers and Aβ protofibrils/fibrils or Aβ dimers and other loMWAβ species represent the predominant Aβ aggregates in the native soluble fraction of the AD brain. SDS-PAGE was used to study the effect of protein denaturation on the spectrum of loMWAβ and hiMWAβ species.

Materials and methods

Neuropathology and human sample characterization

A sample including six AD and four control cases was studied (Table 1). All autopsy brains were collected from individuals who died in the University Hospitals of Bonn or Ulm (Germany). All human tissue was obtained and processed in compliance with German federal laws and with university ethics committee approval.

Demented as well as non-demented patients were examined 1–4 weeks prior to death using standardized protocols for routine clinical examination, including neurological status, upon admission to hospital. These data were used to determine whether individuals clinically fulfilled the DSM-IV criteria for dementia [11]. AD was diagnosed when dementia was observed and when the degree of AD-related neuropathology indicated at least a moderate likelihood for AD according to internationally acknowledged criteria [12].

After assessment of unfixed tissue from one hemisphere for biochemical studies, the brains were fixed in a 4% aqueous formaldehyde solution for at least 3 weeks before undergoing neuropathological screening. Presence or absence of gross infarction, haemorrhage, tumour and other findings were recorded. Tissue blocks from the medial temporal lobe (MTL) were excised at the levels of the (*i*) anterior limit of the dentate gyrus and (*ii*) lateral geniculate body [13]. These blocks together with tissue blocks from the occipital cortex (Brodmann areas 17–19) were embedded in paraffin. All sections were cut at 10 μm.

Neurofibrillary changes were detected by immunostaining with an antibody directed against abnormal phosphorylated τ protein (AT-8, Pierce, Rockford, IL, USA, 1/1000) [14]. Neuritic plaques were also diagnosed in sections immunostained with this same antibody. The presence of Aβ deposition was assessed using immunohistochemistry with an antibody raised against $A\beta_{17-24}$ (4G8 [15], Covance, Emeryville, CA, USA, 1/5000, formic acid pre-treatment).

Diagnosis of the stages in the development of neurofibrillary changes (Braak NFT stage) and the semi-quantitative assessment of neuritic plaques (CERAD score) were performed in accordance with published and recommended criteria [12, 14, 16, 17]. For staging of Aβ pathology, we used a previously published protocol for four phases of β-amyloidosis in the MTL [18]. This hierarchically based procedure facilitates study of the topographic distribution pattern of Aβ deposition in additional brain regions [18, 19]: phase 1 represents Aβ deposition that is restricted to the temporal neocortex. Phase 2 is characterized by the presence of additional Aβ plaques in the entorhinal cortex and/or in the hippocampal subiculum-CA1 region. The third phase is marked by the presence of Aβ plaques in the outer zone of the molecular layer of the fascia dentata, subpial band-like amyloid and/or presubicular 'lake-like' amyloid. The existence of further Aβ plaques in the hippocampal sector CA4 and/or the pre-α layer of the entorhinal cortex characterize the fourth and final phase of Aβ deposition in the MTL. Reference pathology for all cases was performed by one and the same neuropathologist (D.R.T.).

Table 1 List of autopsy cases studied

Case no.	Diagnosis	Age	Gender	AD type	Braak-NFT stage	Aβ phase	CERAD plaque score
1	Control	60	m	0	0	0	0
2	Control	66	m	0	I	0	0
3	Control	69	f	0	I	0	0
4	Control	71	f	0	I	0	0
5	AD	79	f	1	IV	3	2
6	AD	78	m	1	IV	4	1
7	AD	62	f	1	VI	4	3
8	AD	91	f	2	IV	3	1
9	AD	84	m	2	VI	4	3
10	AD	64	f	2	VI	4	3

Ten autopsy cases (four controls, including two females and two males, age range 60–71 years; mean age ± S.D.: 66.5 ± 4.8 years and six AD cases, including four females and two males, age range 62–91 years; mean age ± S.D.: 76.3 ± 11.33 years) were analysed. The table shows neuropathological diagnosis of AD according to published criteria [12], age in years, gender, AD type [10], the stage of neurofibrillary tangle (Braak-NFT stage) pathology according to Braak *et al.* [14, 16], the Aβ-phase representing the distribution of Aβ deposits in subfields of the MTL [18] and the Consortium to Establish a Registry for Alzheimer's Disease (CERAD) score for the frequency of neuritic plaques according to Mirra *et al.* [17]. m: male; f: female; AD: Alzheimer's disease.

Biochemical analysis of human AD and control brains

Fresh frozen human brain tissue from the six AD and four control cases was used to assess the presence and types of native Aβ aggregates in AD and control brains (Table 1). Protein extraction from 30 mg of fresh frozen human occipital (Brodmann areas 17–19) and temporal cortex (Brodmann

areas 35 and 36) was carried out in 2 ml of 0.32 M sucrose dissolved in 1 M Tris-buffer (pH 7.4) with a protease and phosphatase inhibitor cocktail (Complete and PhosSTOP, Roche, Mannheim, Germany). The tissue was homogenized as previously described [20]. The homogenate was placed on ice for 30 min., and the supernatant was clarified by centrifuging for 30 min. at 14,000 × *g* at 4°C. To avoid the segregation of high-molecular weight proteins from the soluble into the insoluble fraction, a centrifuging speed in excess of 14,000 × *g* was not used. The resultant supernatant, *i.e.* the sucrose-soluble fraction, was aliquoted into appropriate volumes and stored at –80°C until use. Protein amounts were determined using BCA Protein Assay (Bio-Rad, Hercules, CA, USA).

For immunoprecipitation, 200 μl of brain lysate was incubated with 1 μl anti-$A\beta_{1-17}$ (6E10, 1 mg/ml; Covance, Dedham, MA, USA), with 20 μl B10AP antibody fragments coupled to alkaline phosphatase ([2], 0.55 mg/ml) or with 1 μl A11 ([6], 1 mg/ml; Millipore, Temecula, CA, USA) antibodies at 4°C for 4 hrs with gentle agitation. A total of 50 μl of protein G Microbeads (Miltenyi Biotec, Bergisch-Gladbach, Germany) were added to the mixture and incubated overnight at 4°C on a shaking table with gentle agitation. The mixture was then passed through the μColumns which separate the microbeads by retaining them into the column, while the rest of the lysate flows through. After several mild rinsing steps with 1× tris-buffered saline (TBS) buffer (pH 7.4), the microbead-bound proteins were eluted with 1× Lithium dodecyl sulfate (LDS) sample buffer at 95°C (Invitrogen, Carlsbad, CA, USA).

For BN-PAGE of the sucrose fraction, 50 μg of total protein was prepared with 4× NativePAGE sample buffer (Invitrogen) and subjected to native PAGE 4–16% Bis-Tris gel electrophoresis according to the manufacturer's protocol (Invitrogen). Native-Mark unstained protein standards (Invitrogen) were used as molecular weight markers. The gel was equilibrated in transfer buffer containing 0.2% SDS for 10 min. After protein transfer onto the nitrocellulose membranes (Bio-Rad), the membrane was boiled in phosphate-buffered saline (PBS) buffer in microwave oven for 6 min. Washing buffer and antibody dilution buffer contained 1 M PBS (pH 7.4) with 0.02% Tween (BioRad). A total of 3% non-fat dry milk (Roth, Karlsruhe, Germany) diluted in antibody-dilution buffer was used to block unspecific binding for 1 hr at room temperature.

For SDS-PAGE, sucrose fractions (50 μg total protein) and immunoprecipitation products were electrophoretically resolved in a precast NuPAGE 4–12% Bis-Tris gel system (Invitrogen). The protein load was controlled either by Ponceau S staining or β-actin (C4, 1/1000; Santa Cruz Biotechnology, Santa Cruz, CA, USA) immunoblotting. The proteins were transferred to nitrocellulose membranes and the membranes were boiled with PBS for 6 min. followed by blocking with 5% non-fat dry milk (Roth; diluted in antibody-dilution buffer) for 1 hr at room temperature.

For immunodetection of the blotted proteins, the membranes were incubated for 24 hrs at 4°C with the primary antibodies: anti-$A\beta_{1-17}$ (6E10, 1/1000), anti-$A\beta_{42}$ (MBC-42, [21] 1/500), anti-$A\beta_{40}$ (MBC-40, [21] 1/1000) and anti-amyloid precursor protein (APP) (22C11, 1/500; Millipore). The 22C11 anti-APP antibody is directed against an N-terminal part of the APP molecule outside the Aβ region [22]. After washing steps, the corresponding secondary antibodies (EIA grade affinity purified goat antimouse/rabbit IgG-HRP, 1/20000; Bio-Rad) were applied for 2 hrs at room temperature. Blots were developed with an enhanced chemiluminescence (ECL) detection system (Supersignal Pico Western system, ThermoScientific-Pierce, Waltham, MA, USA) and illuminated in ECL Hyperfilm (GE Healthcare, Buckinghamshire, UK). $A\beta_{42}$- and $A\beta_{40}$ preparations were used as positive and/or negative controls. All BN-PAGE blots were developed with standard chemiluminescence exposure time of 2–5 min. up to maximum exposure times of 2–3 hrs to detect even minimal amounts of Aβ aggregates. For SDS-PAGE blots, exposure time of 2–5 min. was used except when otherwise indicated.

Electron microscopy of immunoprecipitated oligomeric and fibrillar/protofibrillar proteins from human AD and control brains

For electron microscopy, 5 μl of immunoprecipitated and redissolved A11-positive oligomers or B10AP-positive protofibrils/fibrils were placed on formvar-coated grids. After 1 min. incubation, the excess liquid was wiped off and the grid dried. The grid then was treated with Na-Borhydrite (0.1% in water for 1 min.) followed by blocking with 5% bovine serum albumin, 5% normal goat serum and 0.1% cold-washed fish gelatin in 1 M PBS. The grids were incubated with anti-$A\beta_{1-17}$ (6E10, 1/50) for 30 min. After washing, the primary antibody was visualized by 15 nm gold-labelled secondary antibodies (1/30, diluted in 1 M PBS; Aurion Immuno Gold Reagents & Accessories, Wageningen, The Netherlands). Then, the grid was post-fixed in 2% glutaraldehyde and block-stained with a 2% aqueous solution of uranyl acetate (Merck, Darmstadt, Germany) for 1 min. followed by five rinsing steps in H_2O_2. The sections were viewed with a Philips EM400T 120KV (Eindhoven, The Netherlands) and with a Zeiss EM10 (Oberkochen, Germany).

Analysis of synthetic $A\beta_{42}$ and $A\beta_{40}$ aggregates in native state and after SDS denaturation

To determine whether synthetic Aβ aggregates primarily form loMWAβ- and hiMWAβ aggregates, we dissolved 15 μmol synthetic $A\beta_{40}$-peptide (Peptides International, Louisville, KY, USA) in 1 ml cell culture medium (Quantum 263; PAA Laboratories, Pasching, Austria) for 30 min. at 4°C [23]. $A\beta_{42}$-peptide (Bachem, Bubendorf, Switzerland) was also dissolved in cell culture medium (RPMI1640; GIBCO, Invitrogen) [23]. Aggregation was permitted to occur for 4 hrs at 22°C. To identify oligomers, fibrils and protofibrils structurally we used electron microscopy. For this purpose, 5 μl of the $A\beta_{40}$- and $A\beta_{42}$ solutions were placed on a formvar-coated grid for 1 min. before wiping off the excess liquid. The protein-coated grids were block-stained with a 2% aqueous solution of uranyl acetate (Merck).

The protein aggregates were also analysed with BN-PAGE and SDS-PAGE as well as subsequent Western blot analysis using the MBC-40 and MBC-42 antibodies to detect $A\beta_{40}$ and $A\beta_{42}$, respectively. This experiment was repeated five times.

Results

High-molecular weight $A\beta_{42}$ aggregates predominate in native protein preparations of the soluble fraction from human brain lysates

BN-PAGE with subsequent Western blot analysis of the soluble fraction of human AD brain lysates revealed a high-molecular weight anti-$A\beta_{42}$-positive smear >1000 kD in AD cases (Fig. 1A)

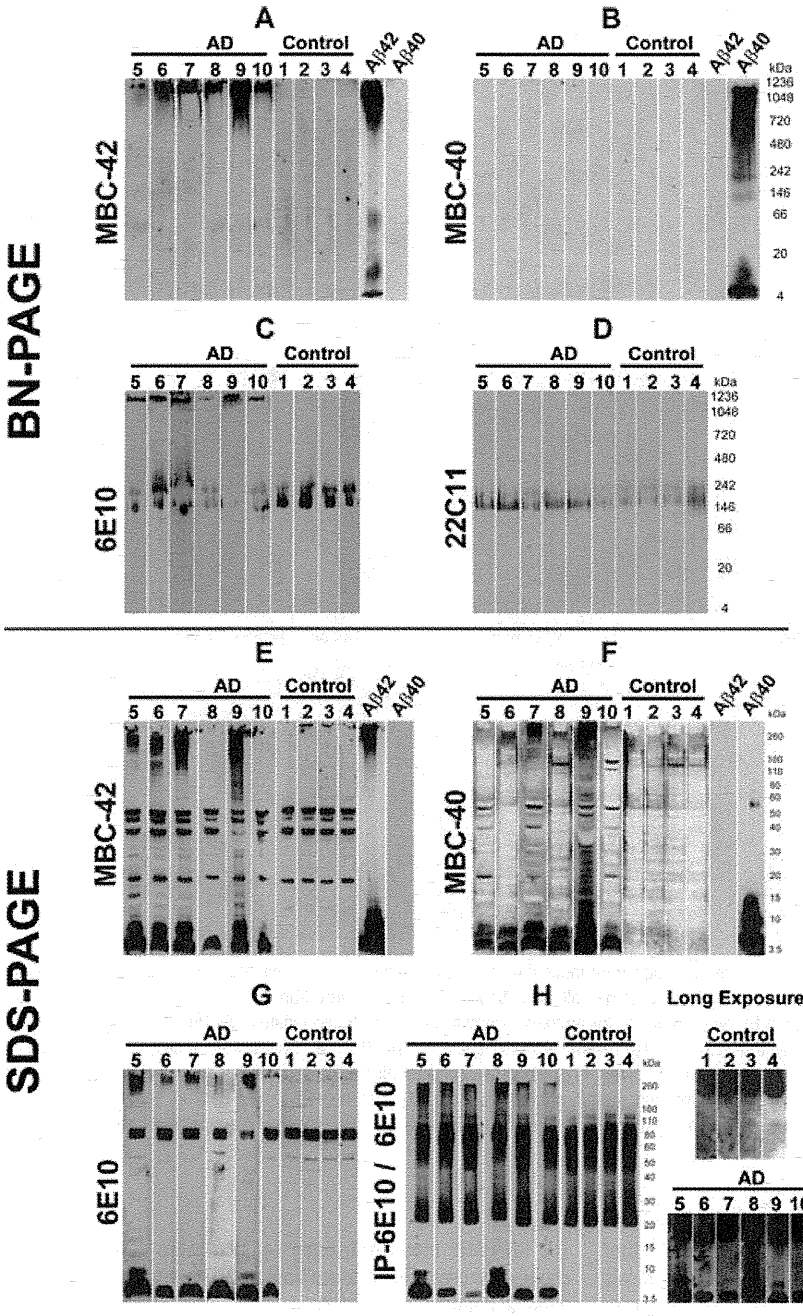

Fig. 1 Western blot analysis of sucrose soluble proteins from AD and control brains after BN-PAGE (**A**–**D**) and after SDS-PAGE (**E**–**H**). All BN-PAGE blots were developed 2–3 hrs for chemiluminescence exposure. SDS-PAGE blots were exposed for 2–5 min. (**A**) The protein lysates from AD brains (cases no. 5–10) in BN-PAGE showed a high-molecular weight anti-$A\beta_{42}$-positive smear >1000 kD. Such smears were not observed in controls (cases no. 1–4). Synthetic $A\beta_{42}$ and $A\beta_{40}$ were loaded as positive and negative controls, respectively. In $A\beta_{42}$ preparations, long chemiluminescence exposure led to the detection of additional dimer and ~50 kD bands that were not observed after 2–5 min. exposures, as shown in Figure 3C. (**B**) The $A\beta_{42}$-positive material seen in (**A**) was not detectable in AD (cases no. 5–10) or in the controls (cases no. 1–4) in the native gel blotted with anti-$A\beta_{40}$ antibodies. Synthetic $A\beta_{42}$ and $A\beta_{40}$ were loaded as positive and negative controls, respectively. After 3 hrs of chemiluminescence exposure, synthetic $A\beta_{40}$ blots display a dimer band at ~10 kD in addition to the monomer band and the hiMWAβ smear already detected with shorter exposure times as depicted in Figure 3C. (**C**) The anti-$A\beta_{1-17}$ antibody also detected the high-molecular weight protein aggregates >1000 kD in the area of stacking gel in the protein lysate from AD brains (cases no. 5–10), which was not detectable in control brains (cases no. 1–4). In addition, anti-$A\beta_{1-17}$ also showed APP bands in AD and control cases (140–240 kD). (**D**) The APP-positive bands were confirmed with an antibody directed against N-terminal epitope of APP (22C11) in control (cases no. 1–4) and AD cases (cases no. 5–10). (**E**)–(**G**) SDS-PAGE analysis of AD brain protein lysates from cases no. 5–10 exhibited Aβ monomer and dimer bands with MBC-42 (**E**), MBC-40 (**F**) and anti-$A\beta_{1-17}$ (**G**) that were not detected in control brains (cases no. 1–4). The MBC-42-dimer (**E**) and 6E10-dimer bands (**G**) were not seen in all AD cases, whereas anti-$A\beta_{40}$ consistently detected dimer bands (**F**). A high-molecular smear was found in most AD cases with all three antibodies directed against Aβ. Interestingly, cases 6 and 10 exhibited nearly no SDS-stable hiMWAβ_{42} aggregates (**E**), whereas both cases showed high-molecular anti-$A\beta_{42}$-positive material in the BN-PAGE (**A**). (**H**) With the help of anti-$A\beta_{1-17}$ (6E10)-immunoprecipitation, monomer and dimer bands as well as loMWAβ (4–20 kD) smears and hiMWAβ (>160 kD) smears were visible in SDS-PAGE of AD brain lysates (cases no. 5–10) but not in those of controls (cases no. 1–4). The detection of the loMWAβ oligomers required chemiluminescence exposure for 3 hrs (*i.e.* long exposure times).

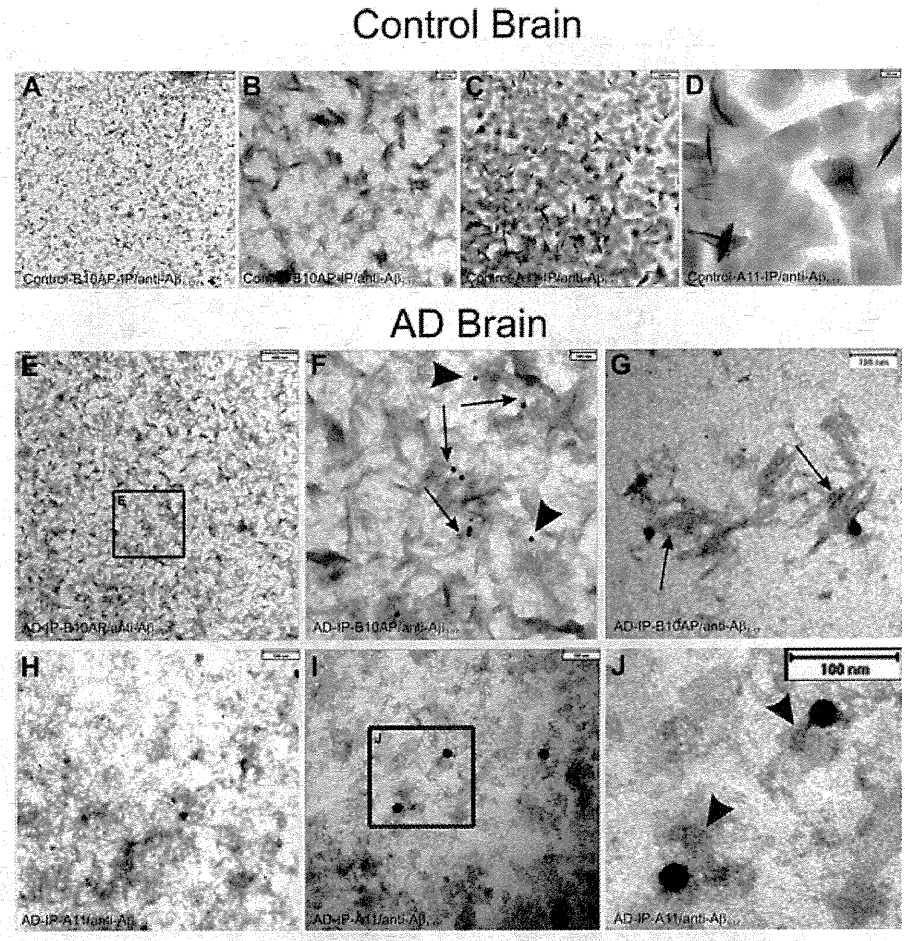

Fig. 2 Electron microscopic analysis of immunoprecipitated protein aggregates from AD and control brain as precipitated with B10AP-antibody fragments (B10AP-IP) and A11 antibodies (A11-IP). (**A**), (**B**) In the control case no. 3, protein aggregates were precipitated with B10AP, but anti-$A\beta_{1-17}$ did not show Aβ within these aggregates. There was also no non-specific labelling with anti-$A\beta_{1-17}$ because no gold particles were observed. The protein aggregates exhibited protofibril-aggregate-like architecture that is more evident at higher magnification (**B**). This indicates that B10AP does not specifically bind to Aβ protofibrils or fibrils but to proteins with a distinct protofibrillar/fibrillar conformation, as reported previously [2]. (**C**), (**D**) A11-IP from control cases resulted in detection of amorphous to spherical presumably oligomeric protein aggregates, as shown in control case no. 4, but did not exhibit Aβ as a component of these protein aggregates. There was also no non-specific labelling with anti-$A\beta_{1-17}$ because no gold particles were seen. The high magnification demonstrates the spherical shape of the precipitated proteins (**D**). Thus, A11 also binds spherical protein aggregates other than Aβ oligomers, as reported earlier by others [6]. (**E**), (**F**) B10AP-IP from AD brain lysate of case no. 7 showed protein aggregates of protofibril-like morphology. Immunogold labelling indicated $A\beta_{1-17}$-positive proteins. The frame in **E** indicates the areas enlarged in (**F**). At higher magnification, $A\beta_{1-17}$-positive material following B10AP-IP exhibited protofibril-like morphology (arrows in **F**) and less frequently amorphous structures (arrowheads in **F**). These types of Aβ aggregates prevailed in B10AP precipitates. (**G**) Only a few precipitated Aβ-positive protein aggregates exhibited fibrillar architecture (case no. 10) resembling synthetic Aβ fibrils (Fig. 3A, B). (**H**) A11-precipitated protein aggregates from AD case no. 7 exhibited spherical to amorphous morphology. Immunogold particles indicate the presence of $A\beta_{1-17}$-positive aggregates. (**I**)–(**J**) Similarly, A11-IP extracted mainly spherical and amorphous protein aggregates from AD case no. 10 shown here at higher magnification. Immunogold labelling indicated $A\beta_{1-17}$-positive proteins. The frame indicates the area enlarged in (**J**). The $A\beta_{1-17}$-positive aggregates observed after A11-IP showed a spherical shape (arrowheads in **J**).

that was not found in controls. Aβ monomers, dimers, or other loMWAβ species were not observed in AD cases or in controls (Fig. 1A). The high-molecular weight smear was also seen with anti-$A\beta_{1-17}$ at the level of stacking gel in AD cases (Fig. 1C) but not with anti-Aβ40 (Fig. 1B). However, the detection of synthetic $A\beta_{40}$ but not $A\beta_{42}$ indicated specific antibody function (Fig. 1B). Anti-$A\beta_{1-17}$ stained an additional 150–250 kD band (Fig. 1C) that was also observable with anti-APP antibodies, thereby indicating that this band represents APP-containing material (Fig. 1D). The APP-related band was also present in control cases, whereas the high-molecular weight anti-$A\beta_{1-17}$ smear was not seen (Fig. 1C). The BN-PAGE blots from brain samples were developed with a chemiluminescence exposure time of 2–3 hrs to detect even very minimal amounts of proteins.

SDS-PAGE with subsequent anti-$A\beta_{42}$, anti-$A\beta_{40}$ and anti-$A\beta_{1-17}$ Western blot analysis showed Aβ monomers and dimers in AD cases (Fig. 1E–G). Aβ aggregates with a molecular weight of >160 kD were observed in four of six cases with anti-$A\beta_{42}$ and a smear >260 kD was observed in all cases with anti-$A\beta_{1-17}$ (6E10) (Fig. 1E–G). After immunoprecipitation with anti-$A\beta_{1-17}$, a smear of hiMWAβ- (>160 kD) and loMWAβ aggregates (8–20 kD) as well as dimer bands at ~10 kD were consistently seen in AD

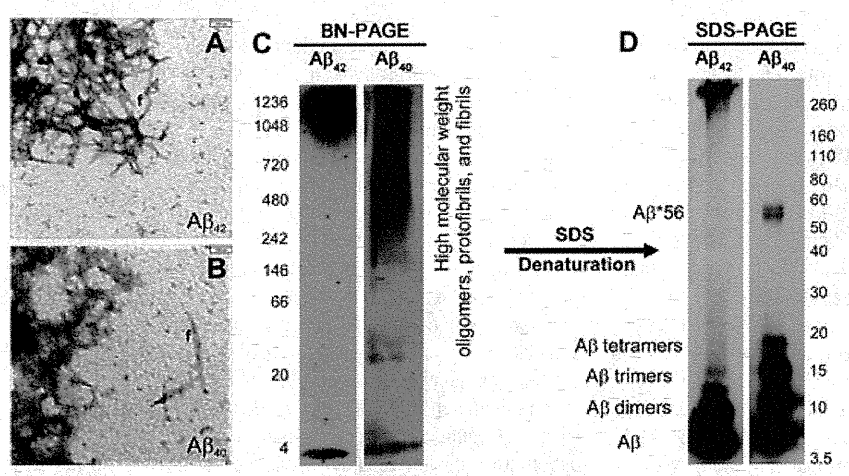

Fig. 3 Synthetic Aβ42 (**A**) and synthetic Aβ40 (**B**) dissolved in cell culture medium aggregated to amorphous oligomers, protofibrils and fibrils (f), as detectable by electron microscopy. (**C**) In BN-PAGE, a high-molecular weight smear occurred mainly above 700 kD in Aβ42 preparations in addition to a distinct monomeric band at ~4 kD. Aβ40 preparations produced a smear of Aβ aggregates with a molecular weight above 242 kD in addition to a clear monomeric band at ~4 kD. The BN-PAGE blots were developed with standard chemiluminescence exposure time of 2–5 min. Longer chemiluminescence exposure for 3 hrs resulted in additional loMWAβ bands depicted in Figure 1A and B, thereby indicating that these preparations contain low levels of these Aβ species as well. (**D**) In SDS-PAGE, hiMWAβ42 aggregates were strikingly reduced. Instead, the monomer, dimer and trimer bands displayed strong staining. Other loMWAβ42 oligomers were not evident. No hiMWAβ40 aggregates were seen after denaturing SDS-PAGE, but Aβ40 monomer, dimer, trimer and tetramer bands as well as an Aβ*56 band were detectable at 56 kD.

cases (Fig. 1H). LoMWAβ and dimers were detected only after 3 hrs of chemiluminescence exposure but not in controls (Fig. 1H).

A11-antibody and B10AP-antibody fragments precipitate oligomeric and protofibrillar/fibrillar proteins including Aβ oligomers, Aβ protofibrils and Aβ fibrils in AD cases

In controls, immunoelectron microscopy of A11- and B10AP-precipitated proteins revealed a high number of precipitated and aggregated proteins that did not contain Aβ-positive material (Fig. 2A–D). There was no nonspecific labelling with anti-Aβ1–17 in controls. B10AP-precipitated material exhibited a pattern that showed fibril-/ protofibril-like architectures (Fig. 2A, B) whereas the proteins precipitated by A11 displayed a spherical pattern (Fig. 2C, D).

In B10AP precipitates of the soluble fraction of AD brain homogenates, we observed protein aggregates with a fibril/protofibril-like pattern similar to that seen in controls. However, in AD brains a high number of Aβ-positive protein aggregates were detected with anti-Aβ1–17 (Fig. 2E–G). High-magnification analysis of anti-Aβ1–17-labeled protein aggregates revealed a protofibril-like pattern (Fig. 2F, arrows). However, a few amorphous protein aggregates (Fig. 2F, arrowheads) as well as fibrillar aggregates (Fig. 2G) were seen as well. Spherical Aβ oligomers were not observed following B10AP immunoprecipitation. Amorphous and spherical protein aggregates were observed after A11-immunoprecipitation from AD brain lysates. Anti-Aβ1–17 antibodies detected protein aggregates of spherical and amorphous morphology (Fig. 2H–J). Protofibril-like structures as seen in B10AP precipitates were not observed in A11 precipitates.

SDS treatment destroys native high-molecular weight Aβ42 and Aβ40 aggregates

Synthetic Aβ42 and Aβ40 formed oligomeric and protofibrillar aggregates as detectable by electron microscopy (Fig. 3A, B). With 2–5 min. chemiluminescence exposure time, BN-PAGE blots revealed a monomer band and an additional prominent smear of Aβ42- and Aβ40 aggregates with a molecular weight >700 and 240 kD, respectively (Fig. 3C). However, after longer exposure time of 2–3 hrs, we observed smeary bands at ~10 and ~50 kD in Aβ42 preparations, whereas Aβ40 preparations exhibited an additional dimer band that was not detectable in short chemiluminescence exposure blots (Figs 1A, B, 3C). In SDS-PAGE, we observed few high-molecular weight aggregates above 240 kD in Aβ42 preparations but not in Aβ40 preparations, whereas very prominent Aβ monomer, dimer and trimer bands were observed for both synthetic Aβ42- and Aβ40 preparations. In SDS-treated Aβ40 preparations, tetramer and Aβ*56 bands were present that were not seen in SDS-treated Aβ42 preparations (Fig. 3D).

Discussion

Our results show that hiMWAβ42 oligomers and protofibrils with a molecular weight >1000 kD predominate in the soluble fraction of AD brain homogenates when these samples are analysed under native BN-PAGE conditions. Aβ40 aggregates were not detected following BN-PAGE. Immunoelectron microscopy of immunoprecipitated oligomeric, fibrillar and protofibrillar proteins confirmed the presence of protofibrillar and spherical hiMWAβ aggregates in the soluble fraction of AD brain homogenates. These hiMWAβ

aggregates were not seen in controls, whereas analysis of control cases revealed that the A11 and B10AP antibodies/antibody fragments precipitate other proteins of similar morphology, and that only a portion of the precipitated proteins from AD cases were Aβ aggregates. Denaturation of the hiMWAβ aggregates by SDS resulted in the detection of Aβ monomers, dimers, and hiMWAβ with a molecular weight >160 kD in SDS-PAGE analysis of AD cases but not in controls. When using immunoprecipitation with anti-$A\beta_{1-17}$, a smear of loMWAβ and hiMWAβ was consistently seen following SDS-PAGE and subsequent Western blot analysis, thus indicating that dimers, trimers, tetramers and Aβ*56 are not the only Aβ oligomers that can be detected with SDS-PAGE as shown previously by other groups as well [4, 5]. These results lead us to conclude that, under native conditions, Aβ monomers and loMWAβ aggregates, such as dimers, trimers and Aβ*56, do not represent the major pool of Aβ aggregates in the human AD brain. More likely, loMWAβ aggregates may occur transiently during aggregation or after denaturation of hiMWAβ. The strongest argument in favour of this hypothesis is our finding that hiMWAβ oligomer preparations and Aβ protofibril preparations of synthetic $A\beta_{42}$- and $A\beta_{40}$ peptides did not exhibit high levels of loMWAβ oligomers in BN-PAGE but did so in SDS-PAGE. Moreover, subsequent to SDS-induced protein denaturation, $hiMWA\beta_{40}$ aggregates were no longer seen and synthetic $hiMWA\beta_{42}$ aggregates were remarkably reduced. A possible argument against the predominance of hiMWAβ in the soluble fraction is that Aβ monomers tend to aggregate in the presence of oligomers [24] and that this occurs during protein preparation. Nevertheless, in synthetic Aβ preparations with high amounts of aggregated Aβ, we detected a significant monomer band after BN-PAGE. This may indicate that Aβ monomers in the soluble brain lysates remained stable during the process of native protein preparation. As such, it is likely that the $hiMWA\beta_{42}$ aggregates observed in the native soluble fraction indeed represent the major form of soluble Aβ in the human AD brain.

Our finding that $A\beta_{40}$ was detected in AD cases in SDS-PAGE but not in BN-PAGE could be attributable either to a lower resolution of native gels in comparison to that of denaturing gels or to the fact that a potential smear of $A\beta_{40}$ aggregates falls far below detectable levels. Presumably, SDS treatment denatures all kinds of $A\beta_{40}$ oligomers and, in so doing, leads to the accumulation of $A\beta_{40}$ monomers in a single band. Thus, a non-detectable $A\beta_{40}$ smear in BN-PAGE might be converted into a detectable well-defined band in the SDS-PAGE. This hypothesis is supported by our finding of a detectable $hiMWA\beta_{40}$ smear in synthetic $A\beta_{40}$ preparation that disappeared after SDS treatment and converted into strongly stained monomer and loMWAβ oligomer bands. In BN-PAGE, the spectrum of synthetic $hiMWA\beta_{40}$ oligomers was greater (>240 kD) than that of synthetic $hiMWA\beta_{42}$ oligomers (>700 kD). This suggests that the concentrations of distinct $hiMWA\beta_{40}$ oligomers are lower than those of distinct $hiMWA\beta_{42}$ oligomers because of the more widespread distribution of $hiMWA\beta_{40}$ aggregates in the gel. As a result, $hiMWA\beta_{40}$ oligomers and may be less easily detected in native brain lysates. An alternative explanation, on the other hand, could be that $A\beta_{40}$ interacts with other proteins that hide its C-terminus. In addition, the predominance of $hiMWA\beta_{42}$ in the native soluble fraction of the AD brains investigated here confirms previous reports of a predominant occurrence of $A\beta_{42}$ in parenchymal soluble and insoluble Aβ aggregates in AD [25, 26].

At first, the results reported here appear to contradict the findings of other authors, who argue that distinct loMWAβ oligomers, such as dimers and Aβ*56, are critical for the development of AD [3, 9, 27]. These authors provide evidence that loMWAβ oligomer preparations received by size-exclusion chromatography are detectable in human as well as transgenic mouse brains, and are capable of inducing cognitive deficits in the rat [9] or altering long-term potentiation [3]. Given our *in vitro* and *in vivo* findings, however, one could also speculate that small amounts of loMWAβ oligomers (possibly resulting from the denaturation of hiMWAβ oligomers, protofibrils and fibrils) either are critical for the development of AD or that, upon their administration, loMWAβ oligomers may spontaneously aggregate and form hiMWAβ oligomers, as appears to be the case based upon our native gel analysis of $A\beta_{40}$- and $A\beta_{42}$ preparations and the results of Nguyen *et al.* [24], who showed that Aβ oligomers accommodate added Aβ monomers. Thus, hiMWAβ aggregates contribute to the pathogenesis of AD either on its own or do so indirectly by providing the reservoir of hiMWAβ aggregates that denature and, in so doing, release loMWAβ oligomers.

That Aβ aggregates, including Aβ plaques, dissociate during the pathogenesis of AD is corroborated by the finding that in late-stage AD cases plaque frequency is lower than in earlier stages [28]. The relevance of soluble hiMWAβ for the pathogenesis of AD may be further supported by the finding of neuritic degeneration near Aβ plaques, *i.e.* in areas with high levels of hiMWAβ presumably dissolved from Aβ plaques, in the APP transgenic mouse brain [7, 8, 29], in aged rhesus monkeys [30] and in the AD brain [31], and also by the finding that dendritic degeneration in another APP-transgenic mouse model begins at the same time as the deposition of initial diffuse Aβ-plaques, *i.e.* when hiMWAβ aggregates begin to predominate in the cortex [32].

Here, the stability of $hiMWA\beta_{42}$ aggregates was greater than that of $A\beta_{40}$ aggregates in *in vitro* experiments, thus confirming previous reports that soluble $A\beta_{42}$ aggregates are more stable than $A\beta_{40}$ aggregates [33, 34]. Taken together with our finding that $hiMWA\beta_{42}$ aggregates predominate in the native soluble fraction of the brain, it may be speculated that it is the stability of soluble $A\beta_{42}$ aggregates in the soluble compartment of the brain that accounts for its predominance in parenchymal Aβ plaque deposition [26].

In conclusion, the results of the present study strongly suggest that hiMWAβ oligomers, protofibrils and fibrils are the predominant soluble Aβ aggregates in the AD brain. loMWAβ oligomers in high concentrations are detectable only after denaturation of hiMWAβ aggregates. In view of the denaturation of hiMWAβ aggregates and fibrils into loMWAβ oligomers, we propose that Aβ plaques consisting of both fibrillar Aβ as well as soluble

hiMWAβ aggregates may serve as reservoirs for the release of loMWAβ oligomers.

Acknowledgement

We thank Kelly Del Tredici, M.D., Ph.D. (University of Ulm, Department of Neurology, Center for Clinical Research) for reading the final version of the revised manuscript.

Conflict of interest

D.R.T. received research grants from the Deutsche Forschungsgemeinschaft (DFG-grant TH624/6–1) and from the Alzheimer Forschung Initiative (AFI Grant #10810). M.F. was supported by the Deutsche Forschungsgemeinschaft (SFB 610) and the Landesexzellenz-Netzwerk Biowissenschaften. There are no other conflicts of interest.

References

1. **Masters CL, Simms G, Weinman NA, *et al.*** Amyloid plaque core protein in Alzheimer disease and Down syndrome. *Proc Natl Acad Sci USA.* 1985; 82: 4245–9.
2. **Habicht G, Haupt C, Friedrich RP, *et al.*** Directed selection of a conformational antibody domain that prevents mature amyloid fibril formation by stabilizing Abeta protofibrils. *Proc Natl Acad Sci USA.* 2007; 104: 19232–7.
3. **Shankar GM, Li S, Mehta TH, *et al.*** Amyloid-beta protein dimers isolated directly from Alzheimer's brains impair synaptic plasticity and memory. *Nat Med.* 2008; 14: 837–42.
4. **Rosen RF, Ciliax BJ, Wingo TS, *et al.*** Deficient high-affinity binding of Pittsburgh compound B in a case of Alzheimer's disease. *Acta Neuropathol.* 2010; 119: 221–33.
5. **Rosen RF, Tomidokoro Y, Ghiso JA, *et al.*** SDS-PAGE/immunoblot detection of Abeta multimers in human cortical tissue homogenates using antigen-epitope retrieval. *J Vis Exp.* 2010; 38: doi: 10.3791/1916.
6. **Kayed R, Head E, Thompson JL, *et al.*** Common structure of soluble amyloid oligomers implies common mechanism of pathogenesis. *Science.* 2003; 300: 486–9.
7. **Spires TL, Meyer-Luehmann M, Stern EA, *et al.*** Dendritic spine abnormalities in amyloid precursor protein transgenic mice demonstrated by gene transfer and intravital multiphoton microscopy. *J Neurosci.* 2005; 25: 7278–87.
8. **Tsai J, Grutzendler J, Duff K, *et al.*** Fibrillar amyloid deposition leads to local synaptic abnormalities and breakage of neuronal branches. *Nat Neurosci.* 2004; 7: 1181–3.
9. **Lesne S, Koh MT, Kotilinek L, *et al.*** A specific amyloid-beta protein assembly in the brain impairs memory. *Nature.* 2006; 440: 352–7.
10. **Thal DR, Papassotiropoulos A, Saido TC, *et al.*** Capillary cerebral amyloid angiopathy identifies a distinct APOE epsilon4-associated subtype of sporadic Alzheimer's disease. *Acta Neuropathol.* 2010; 120: 169–83.
11. **American Psychiatric Association.** Diagnostic and statistical manual of mental disorders. 4th ed. Washington DC: American Psychiatric Association; 1994.
12. **The National Institute on Aging.** Consensus recommendations for the postmortem diagnosis of Alzheimer's disease. The National Institute on Aging, and Reagan Institute Working Group on Diagnostic Criteria for the Neuropathological Assessment of Alzheimer's Disease. *Neurobiol Aging.* 1997; 18: S1–2.
13. **Insausti R, Amaral DG.** Hippocampal Formation. In: Paxinos G, Mai JK, editors. The human nervous system. 2nd ed. London: Elsevier; 2004. pp. 872–914.
14. **Braak H, Alafuzoff I, Arzberger T, *et al.*** Staging of Alzheimer disease-associated neurofibrillary pathology using paraffin sections and immunocytochemistry. *Acta Neuropathol.* 2006; 112: 389–404.
15. **Kim KS, Miller DL, Sapienza VJ, *et al.*** Production and characterization of monoclonal antibodies reactive to synthetic cerebrovascular amyloid peptide. *Neurosci Res Commun.* 1988; 2: 121–30.
16. **Braak H, Braak E.** Neuropathological stageing of Alzheimer-related changes. *Acta Neuropathol.* 1991; 82: 239–59.
17. **Mirra SS, Heyman A, McKeel D, *et al.*** The Consortium to Establish a Registry for Alzheimer's Disease (CERAD). Part II. Standardization of the neuropathologic assessment of Alzheimer's disease. *Neurology.* 1991; 41: 479–86.
18. **Thal DR, Rüb U, Schultz C, *et al.*** Sequence of Abeta-protein deposition in the human medial temporal lobe. *J Neuropathol Exp Neurol.* 2000; 59: 733–48.
19. **Thal DR, Rüb U, Orantes M, *et al.*** Phases of Abeta-deposition in the human brain and its relevance for the development of AD. *Neurology.* 2002; 58: 1791–800.
20. **Utter S, Tamboli IY, Walter J, *et al.*** Cerebral small vessel disease-induced apolipoprotein E leakage is associated with Alzheimer disease and the accumulation of amyloid beta-protein in perivascular astrocytes. *J Neuropathol Exp Neurol.* 2008; 67: 842–56.
21. **Yamaguchi H, Sugihara S, Ogawa A, *et al.*** Diffuse plaques associated with astroglial amyloid beta protein, possibly showing a disappearing stage of senile plaques. *Acta Neuropathol.* 1998; 95: 217–22.
22. **Weidemann A, Konig G, Bunke D, *et al.*** Identification, biogenesis, and localization of precursors of Alzheimer's disease A4 amyloid protein. *Cell.* 1989; 57: 115–26.
23. **Huang X, Atwood CS, Moir RD, *et al.*** Trace metal contamination initiates the apparent auto-aggregation, amyloidosis, and oligomerization of Alzheimer's Abeta peptides. *J Biol Inorg Chem.* 2004; 9: 954–60.
24. **Nguyen PH, Li MS, Stock G, *et al.*** Monomer adds to preformed structured oligomers of Abeta-peptides by a two-stage dock-lock mechanism. *Proc Natl Acad Sci USA.* 2007; 104: 111–6.
25. **Murphy MP, Beckett TL, Ding Q, *et al.*** Abeta solubility and deposition during AD progression and in APPxPS-1 knock-in mice. *Neurobiol Dis.* 2007; 27: 301–11.
26. **Roher AE, Lowenson JD, Clarke S, *et al.*** beta-Amyloid-(1–42) is a major component of cerebrovascular amyloid deposits: implications for the pathology of Alzheimer disease. *Proc Natl Acad Sci USA.* 1993; 90: 10836–40.
27. **Reed MN, Hofmeister JJ, Jungbauer L, *et al.*** Cognitive effects of cell-derived and synthetically derived Abeta oligomers.

Neurobiol Aging. 2009: doi:10.1016/j.neurobiolaging.2009.11.007.

28. **Thal DR, Arendt T, Waldmann G, *et al.*** Progression of neurofibrillary changes and PHF-tau in end-stage Alzheimer's disease is different from plaque and cortical microglial pathology. *Neurobiol Aging.* 1998; 19: 517–25.
29. **Meyer-Luehmann M, Spires-Jones TL, Prada C, *et al.*** Rapid appearance and local toxicity of amyloid-beta plaques in a mouse model of Alzheimer's disease. *Nature.* 2008; 451: 720–4.
30. **Shah P, Lal N, Leung E, *et al.*** Neuronal and Axonal Loss Are Selectively Linked to Fibrillar Amyloid-{beta} within Plaques of the Aged Primate Cerebral Cortex. *Am J Pathol.* 2010; 177: 325–33.
31. **Serrano-Pozo A, William CM, Ferrer I, *et al.*** Beneficial effect of human anti-amyloid-beta active immunization on neurite morphology and tau pathology. *Brain.* 2010; 133: 1312–27.
32. **Capetillo-Zarate E, Staufenbiel M, Abramowski D, *et al.*** Selective vulnerability of different types of commissural neurons for amyloid beta-protein induced neurodegeneration in APP23 mice correlates with dendritic tree morphology. *Brain.* 2006; 129: 2992–3005.
33. **Lambert MP, Barlow AK, Chromy BA, *et al.*** Diffusible, nonfibrillar ligands derived from Abeta1–42 are potent central nervous system neurotoxins. *Proc Natl Acad Sci USA.* 1998; 95: 6448–53.
34. **Levine H 3rd.** Soluble multimeric Alzheimer beta(1–40) pre-amyloid complexes in dilute solution. *Neurobiol Aging.* 1995; 16: 755–64.

THE JOURNAL OF BIOLOGICAL CHEMISTRY VOL. 287, NO. 9, pp. 6912–6927, February 24, 2012
Published in the U.S.A.

Tannic Acid Is a Natural β-Secretase Inhibitor That Prevents Cognitive Impairment and Mitigates Alzheimer-like Pathology in Transgenic Mice*

Received for publication, August 15, 2011, and in revised form, December 20, 2011 Published, JBC Papers in Press, January 4, 2012, DOI 10.1074/jbc.M111.294025

Takashi Mori,[a,b1] **Kavon Rezai-Zadeh,**[c] **Naoki Koyama,**[a] **Gary W. Arendash,**[d,e] **Haruyasu Yamaguchi,**[f] **Nobuto Kakuda,**[g] **Yuko Horikoshi-Sakuraba,**[g] **Jun Tan,**[h,i] **and Terrence Town**[c,j,k2]

From the Departments of [a]Biomedical Sciences and [b]Pathology, Saitama Medical Center and University, Kawagoe, Saitama 350-8550, Japan, the [c]Department of Biomedical Sciences and Regenerative Medicine Institute Neural Program and the [j]Department of Neurosurgery, Maxine Dunitz Neurosurgical Institute, Cedars-Sinai Medical Center, Los Angeles, California 90048, the [d]Florida Alzheimer's Disease Research Center and the [e]Department of Cell Biology, Microbiology, and Molecular Biology, University of South Florida, Tampa, Florida 33620, the [f]Gunma University School of Health Sciences, Maebashi, Gunma 371-8514, Japan, the [g]Immuno-Biological Laboratories Co., Ltd., Fujioka, Gunma 375-0005, Japan, the [h]Rashid Laboratory for Developmental Neurobiology, Silver Child Development Center and the [i]Neuroimmunology Laboratory, the Department of Psychiatry and Neurosciences, College of Medicine, University of South Florida, Tampa, Florida 33613, and the [k]Department of Medicine, David Geffen School of Medicine, University of California, Los Angeles, California 90048

Background: Recent focus has been given to anti-amyloidogenic naturally occurring polyphenols known as flavonoids.
Results: The polyphenol tannic acid prevented behavioral impairment and mitigated Alzheimer disease-like pathology.
Conclusion: Tannic acid may be prophylactic for Alzheimer disease by inhibiting β-secretase activity and mitigating brain pathology.
Significance: This nutraceutical approach offers a new class of drug for inhibiting β-secretase with few if any side effects.

Amyloid precursor protein (APP) proteolysis is essential for production of amyloid-β (Aβ) peptides that form β-amyloid plaques in brains of Alzheimer disease (AD) patients. Recent focus has been directed toward a group of naturally occurring anti-amyloidogenic polyphenols known as flavonoids. We orally administered the flavonoid tannic acid (TA) to the transgenic PSAPP mouse model of cerebral amyloidosis (bearing mutant human APP and presenilin-1 transgenes) and evaluated cognitive function and AD-like pathology. Consumption of TA for 6 months prevented transgene-associated behavioral impairment including hyperactivity, decreased object recognition, and defective spatial reference memory, but did not alter nontransgenic mouse behavior. Accordingly, brain parenchymal and cerebral vascular β-amyloid deposits and abundance of various Aβ species including oligomers were mitigated in TA-treated PSAPP mice. These effects occurred with decreased cleavage of the β-carboxyl-terminal APP fragment, lowered soluble APP-β production, reduced β-site APP cleaving enzyme 1 protein stability and activity, and attenuated neuroinflammation. As *in vitro* validation, we treated well characterized mutant human APP-overexpressing murine neuron-like cells with TA and found significantly reduced Aβ production associated with less amyloidogenic APP proteolysis. Taken together, these results raise the possibility that dietary supplementation with TA may be prophylactic for AD by inhibiting β-secretase activity and neuroinflammation and thereby mitigating AD pathology.

Alzheimer disease (AD)[3] is the most common dementia and is a growing worldwide public health concern (1). AD neuropathological hallmarks include extracellular deposits of amyloid-β (Aβ) peptides, intracellular neurofibrillary tangles, neuronal and synaptic degeneration/loss, and neuroinflammation (2). Brain Aβ deposition likely results from increased peptide accumulation/reduced clearance, endorsing toxic events that drive AD pathogenesis (3, 4). Aβ is produced from sequential endoproteolytic cleavage of amyloid precursor protein (APP) by β- and γ-secretases (5–9), and enters a dynamic equilibrium between soluble and deposited forms (10). In recent years, much attention has been directed toward soluble multimeric forms of Aβ peptides as the toxic species. These so-called "Aβ oligomers" disrupt synaptic function and induce neurotoxicity *in vivo* (11–13).

* This work was supported, in whole or in part, by National Institutes of Health Grants 5R00AG029726-04, 3R00AG029726-04S1, and 1R01NS076794-01 from the NIA and the NINDS (to T. T.), Grant-in-aid for Scientific Research (C) 22500320 (to T. M.) from the Japan Society for the Promotion of Science and Grant-in-aid for Scientific Research (B) 19300122 (to H. Y.) from the Ministry of Education, Culture, Sports, Science and Technology, Alzheimer's Association Zenith Fellows Award ZEN-10-174633 (to T. T.), and American Federation of Aging Research/Ellison Medical Foundation Julie Martin Mid-Career Award in Aging Research M11472 (to T. T.).

[1] To whom correspondence may be addressed. Tel.: 81-49-228-3592; E-mail: t_mori@saitama-med.ac.jp.

[2] Inaugural holder of the Ben Winters Endowed Chair in Regenerative Medicine. To whom correspondence may be addressed: Regenerative Medicine Institute, Cedars-Sinai Medical Center, 8700 Beverly Blvd., Steven Spielberg Building, Rm. 361, Los Angeles, CA 90048. Tel.: 310-248-8581; E-mail: terrence.town@cshs.org.

[3] The abbreviations used are: AD, Alzheimer disease; CTF, carboxyl-terminal fragment; APP, amyloid precursor protein; Aβ, amyloid-β; BACE1, β-site APP cleaving enzyme 1; CAA, cerebral amyloid angiopathy; EGCG, (−)-epigallocatechin-3-gallate; TA, tannic acid; Iba1, ionized calcium-binding adapter molecule 1; GFAP, glial fibrillary acidic protein; QPCR, quantitative real-time PCR; ANOVA, analysis of variance; CC, cingulate cortex; H, hippocampus; EC, entorhinal cortex; sAPP, soluble APP.